Solar-Induced Chlorophyll Fluorescence (SIF): Towards a Better Understanding of Vegetation Dynamics and Carbon Uptake in Arctic-Boreal Ecosystems

Current Climate Change Reports
https://doi.org/10.1007/s40641-024-00194-8

REVIEW

Solar-Induced Chlorophyll Fluorescence (SIF): Towards a Better Understanding of Vegetation Dynamics and Carbon Uptake in Arctic-Boreal Ecosystems

Rui Cheng[1,2]

Accepted: 28 February 2024

Abstract

Purpose of Review Terrestrial ecosystems in the Arctic-Boreal region play a crucial role in the global carbon cycle as a carbon sink. However, rapid warming in this region induces uncertainties regarding the future net carbon exchange between land and the atmosphere, highlighting the need for better monitoring of the carbon fluxes. Solar-Induced chlorophyll Fluorescence (SIF), a good proxy for vegetation CO^2 uptake, has been broadly utilized to assess vegetation dynamics and carbon uptake at the global scale. However, the full potential and limitations of SIF in the Arctic-Boreal region have not been explored. Therefore, this review aims to provide a comprehensive summary of the latest insights into Arctic-Boreal carbon uptake through SIF analyses, underscoring the advances and challenges of SIF in solving emergent unknowns in this region. Additionally, this review proposes applications of SIF across scales in support of other observational and modeling platforms for better understanding Arctic-Boreal vegetation dynamics and carbon fluxes.

Recent Findings Cross-scale SIF measurements complement each other, offering valuable perspectives on Arctic-Boreal ecosystems, such as vegetation phenology, carbon uptake, carbon-water coupling, and ecosystem responses to disturbances. By incorporating SIF into land surface modeling, the understanding of Arctic-Boreal changes and their climate drivers can be mechanistically enhanced, providing critical insights into the changes of Arctic-Boreal ecosystems under global warming.

Summary While SIF measurements are more abundant and with finer spatiotemporal resolutions, it is important to note that the coverage of these measurements is still limited and uneven in the Arctic-Boreal region. To address this limitation and further advance our understanding of the Arctic-Boreal carbon cycle, this review advocates for fostering a SIF network providing long-term and continuous measurements across spatial scales. Simultaneously measuring SIF and other environmental variables in the context of a multi-modal sensing system can help us comprehensively characterize Arctic-Boreal ecosystems with spatial details in land surface models, ultimately contributing to more robust climate projections.

Keywords Solar-Induced chlorophyll Fluorescence (SIF) · The Arctic-Boreal region · Carbon uptake · Modeling

Background

Terrestrial ecosystems in the Arctic-Boreal region play a critical role in the global carbon cycle and climate change mitigation as a significant net carbon sink through vegetation photosynthesis [1, 2]. Based on the Coupled Model Intercomparison Project Phase 6 (CMIP6; [3]), a tipping point of the carbon cycle is projected with reduced net sink in the Arctic-Boreal region by the end of the 21st century and potentially to turn the region into a net carbon source in the next century [4, 5]. This weaker net carbon sink can be attributed to unique consequences of rapid warming in this region [6], which have divergent impact on photosynthesis. For example, (1) thawing permafrost enhances microbial decomposition, while it may favor photosynthetic carbon uptake through enriched soil nutrients [7–9]; (2) more frequent and widespread fires [10–12] rapidly clear vegetation coverage and release large amounts of carbon into the atmosphere reversing decades of carbon uptake [13, 14]; and

✉ Rui Cheng
ruicheng@umn.edu; rccheng@mit.edu

1 Department of Bioproducts and Biosystems Engineering, University of Minnesota, 1390 Eckles Ave., St. Paul, Minneapolis, MN 55108, USA

2 Department of Civil and Environmental Engineering, Massachusetts Institute of Technology, 15 Vassar Street, Cambridge, MA 02139, USA

(3) shifts of plant compositions [15–17], plant productivity [18, 19], and plant phenology [20–22] lead to heterogeneous changes in carbon uptake [23–25]. Due to complex and understudied ecosystem-climate feedbacks [26–33], the carbon uptake by photosynthesis at the ecosystem level, which is also known as Gross Primary Productivity (GPP), is highly uncertain in this region. Compared to the 24% uncertainty of global GPP (3.3 ± 0.8 gt C yr^{-1}; [34]), the uncertainty of Arctic-Boreal GPP is 227% of its typical value (0.22 ± 0.50 kg C m^{-2} yr^{-1}), becoming the second largest uncertainty source for the carbon cycle [35]. Therefore, to better understand the ecosystem-climate feedbacks in the Arctic-Boreal region and constrain the uncertainties on the global carbon cycle [36, 37], there is a pressing need to closely monitor GPP [5, 38, 39].

GPP can be evaluated both directly and remotely. Direct measurements of GPP rely on chamber-based measurements [40, 41] and tower-based Eddy Covariance techniques (EC) [42, 43]. Chamber-based measurements are advantageous at evaluating GPP from different vegetation types within an ecosystem. However, existing chambers in the Arctic-Boreal region are mostly manual and thus laborious [44]. Contrarily, EC averages out fine-scale heterogeneity but provides convenient long-term monitoring [43]. While the state-of-the-art flux product in this region (i.e., ABCflux [39]) synthesizes available chamber-based and EC observations, the representativeness of this product is still limited due to the spatial scarcity and temporal sporadicity of both methods [35, 39, 45, 46], especially compared to growing long-term EC networks in other regions [47–59],

Remote sensing techniques, on the other hand, can infer GPP continuously with extensive spatial coverage [60–64] in spite of some shortfalls unique to the Arctic-Boreal region, such as seasonal gaps of observations and complications from non-vegetation [65, 66]. A conceptual model of remotely inferred GPP can be expressed as:

$$\mathrm{GPP} = \mathrm{fPAR} \times \mathrm{PAR} \times \mathrm{LUE}, \qquad (1)$$

where PAR is Photosynthetic Activate Radiation, and fPAR is the fraction of PAR being absorbed by chlorophyll. The product of fPAR and PAR, that is the Absorbed PAR (APAR), will be primarily partitioned between photochemical quenching for photosynthesis and dissipation of excess energy as heat by photoprotective pigments. A small amount of APAR will be re-emitted in red and far-red wavelengths as Solar-Induced chlorophyll Fluorescence (SIF) [67]. Hence, Light Use Efficiency (LUE) quantifies the fraction of APAR utilized by photosynthesis.

Conventionally, remotely inferred GPP is based on the canopy color measured by optical reflectance because the canopy greenness is a proxy of APAR [64, 68, 69]. The vegetation indices of greenness measurements such as Normalized Difference Vegetation Index (NDVI) [68] and Enhanced Vegetation Index (EVI) [70] are commonly used for this purpose. Nevertheless, canopy greenness alone provides no information about LUE [71, 72]. This limitation of canopy greenness challenges the GPP estimation for land cover types with sustained canopy greenness and APAR, such as evergreen forests which is one of the dominant land cover types in the Arctic-Boreal region [73, 74].

More recently, advancements in remote sensing have revealed that canopy-scale far-red SIF, i.e., far-red SIF escaped from the canopy and detected by remote instruments, serves as a better proxy for GPP than conventional greenness measurements [75, 76]. A conceptual model for instantaneous canopy-scale SIF measurements [77, 78] can be written as:

$$\mathrm{SIF} = \mathrm{fPAR} \times \mathrm{PAR} \times \Phi_F \times f_{\mathrm{esc}}, \qquad (2)$$

where Φ_F is the quantum yield of fluorescence, and f_{esc} is the probability of fluorescence escaping the canopy and reaching the remote instruments [79, 80]. To account for the dependence of SIF on the instantaneous PAR at the time of measurement, the instantaneous SIF measurements are often normalized to daily mean SIF ($\mathrm{SIF_{dc}}$) by solar zenith angle [65, 81–84].

This conceptual model underscores that SIF is primarily driven by APAR as a bi-product of photosynthesis ([76]). Meanwhile, SIF also contains LUE information [75] because Φ_F is under the regulation of photoprotective pigments [85]. These links with APAR and LUE make SIF a critical tool for mechanistically tracking GPP in land cover types with and without persistent canopy greenness. Besides, SIF retrieval is less sensitive to common background noise in the Arctic-Boreal region, such as water and snow [66, 69, 86, 87]. Given these strengths, SIF is an effective tool in the Arctic-Boreal region. Several studies have presented this advantage of SIF over canopy greenness empirically [66, 86, 88–91]. However, the full potential of SIF in evaluating vegetation dynamics and constraining uncertainties on carbon fluxes with spatial details is still underexplored.

There have been a few review articles on SIF [92–94] that extensively discuss observational platforms, retrieval techniques, the physiological link between SIF and photosynthesis at the molecular level and global scale. However, limited by their global scopes, these reviews have not assessed the unique challenges of SIF in the Arctic-Boreal region, such as limited observations and underrepresented land cover types. To advance the application of SIF in the Arctic-Boreal region, this review focuses on recent progress on Arctic-Boreal SIF observations and assessing the prospects of SIF research across the Arctic-Boreal region for better monitoring vegetation dynamics and carbon fluxes in response to climate change.

Cross-scale SIF Measurements

This section aims to comprehensively overview cross-scale instruments used for measuring SIF in the Arctic-Boreal region. Currently, there are only a few studies [66, 95–97] quantitatively analyze the linear proximity of SIF and GPP from different observational platforms (Fig. 1). By examining the advantages and limitations of spaceborne, airborne, and tower-based instruments, their applications can be optimized for capturing the spatial distribution and temporal dynamics of SIF in the Arctic-Boreal region [66, 91, 98].

Spaceborne SIF

Several generations of spaceborne instruments have been deployed to measure SIF across the globe, but not all of them are optimal for the Arctic-Boreal region. Notable satellite missions/instruments overpassing the Arctic-Boreal region (north of 50°N) include the Global Ozone Monitoring Experiment-2 (GOME-2) [99], Greenhouse gases Observing SATellite (GOSAT) [100], SCanning Imaging Absorption spectroMeter for Atmospheric CartograpHY (SCIAMACHY) [101], Orbiting Carbon Observatory-2 (OCO-2) [102], Carbon Dioxide Observation Satellite Mission (TanSat) [103], and TROPOspheric Monitoring Instrument (TROPOMI) [82]. Each satellite mission/instrument has different scanning patterns and satellite orbits, resulting in diverse spatial and temporal characteristics of SIF measurements (Table 1, Fig. 2). Therefore, it is important to consider these differences when comparing their SIF measurements across satellite missions/instruments and inferring GPP from their SIF measurements [98]. To address this issue in the context of Arctic-Boreal ecosystems, common methods of processing SIF measurements will be discussed in this section.

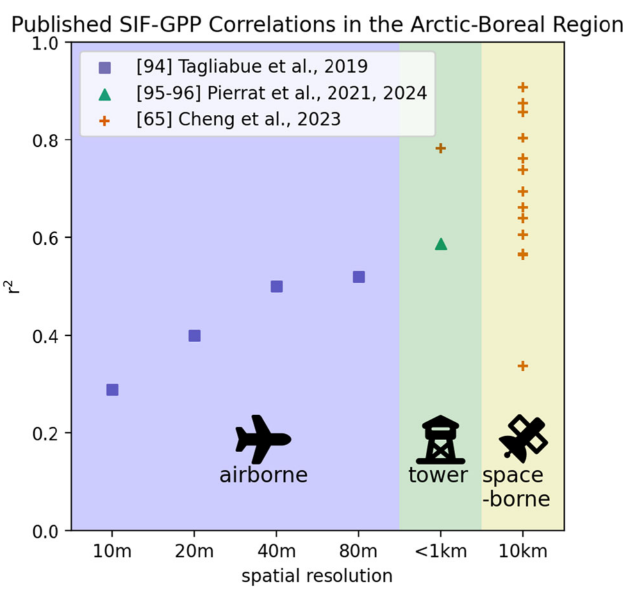

Fig. 1 A graphic summary of published r^2 in the Arctic-Boreal region between GPP and SIF from different observational platforms and spatial resolutions, including an airborne platform with spatial resolutions of 10 m, 20 m, 40 m, and 80 m; tower-based platforms without uniform spatial resolution (Table 2); and a spaceborne platform at 10km resolution. Each scatter represents a study site/spatial resolution. The airborne data points are from the modeled instantaneous GPP and airborne snapshot of SIF [95], while the tower-based and spaceborne data points are from daily mean Eddy Covariance (EC) GPP and daily mean tower/satellite SIF [66, 96, 97]. Cheng et al., [66] reported r^2 based on the climatology, which may not be derived from synced timeseries of GPP and SIF

Spatial Coverage and Resolution

The spatial coverage of satellite missions/instruments determines the geographic range of SIF measurements. Most existing satellites, such as SCIAMACHY, GOME/GOME-2, GOSAT/GOSAT-2, TanSAT, OCO-2, and TROPOMI (Table 1, Fig. 2a), have polar or near-polar orbits that allow for SIF measurements in the Arctic-Boreal region as they pass over the entire latitudinal range of the region. However, certain satellites, namely Tropospheric Emissions: Monitoring Pollution (TEMPO) and Sentinel-4, have limited coverage and primarily focus on lower latitudes of the region, up to 58° N and 65° N, respectively (refer to Table 1 and Fig. 2a). As a result, these satellite missions/instruments will not provide sufficient SIF measurements for the entire Arctic-Boreal region.

The spatial resolution of SIF measurements determines their spatial representativeness relative to the heterogeneous surface in the Arctic-Boreal. Fine spatial resolution is important for the Arctic-Boreal region because the land cover in this region is highly heterogeneous, with the co-existence of different land cover types, such as vegetation, water, and snow [104]. In addition, complex topography poses challenges in resolving these diverse land cover types within large pixels [66, 105, 106]. Coarse spatial resolutions may yield a wide range of correlations between SIF and GPP (Fig. 1). Therefore, SIF measurements with finer spatial resolution have greater potential to represent different land cover types more accurately and distinguish their contributions to the carbon cycle in the Arctic-Boreal region [96, 107, 108]. Also, measurements with lower spatial resolutions (larger pixel sizes) are more susceptible to contaminations from clouds and aerosols, such as SCIAMACHY, GOME/GOME-2, GOSAT/GOSAT-2 [99, 109]. Currently, state-of-the-art satellite missions/instruments like TROPOMI and OCO-2 offer SIF measurements with finer spatial resolutions. Upcoming missions, particularly the European Space Agency's FLuorescence EXplorer (FLEX) [110, 111], will significantly enhance the spatial resolution, with a footprint size of 300 x 300 m^2, which will be the smallest among current SIF measurements (Fig. 2b). It is worth

Table 1 Existing and upcoming satellite missions/instruments measuring SIF in the Arctic-Boreal region (north of 50°N)

Instruments/Satellites	Space		Time	
	Coverage	Resolution	Span	Global Coverage Cycle (Overpass at Equator)
SCIAMACHY/ENVISAT[1]	global	30 x 240 km^2	2003–2012	6 days (10:00 LST)
GOME/ERS-2[2]	global	40 x 320 km^2	1995–2003	3 days (10:30 LST)
GOME-2/MetOp-A[3]	global	40 x 80 km^2 or 40 x 40 km^2	2007–present	1.5 days (9:30 LST)
TANSO-FTS/**GOSAT**[4]	global	10.5km-diameter circular	2010–present	3 days (13:00 LST)
TANSO-FTS/**GOSAT-2**[5]	global	9.7km-diameter circular	2019–present	6 days (13:00 LST)
AGCS/**TanSat**[6]	global	2 x 2 km^2	2017–present	16 days (13:30 LST)
OCO-2[7]	global	1.3 x 2 km^2	2014–present	16 days (13:30 LST)
TROPOMI/Sentinel-5p[9]	global	7 x (3.5–15) km^2	2018–present	1 day (13:30 LST)
FLORIS/**FLEX**[11]	global	300 x 300 m^2	planned for 2025	27 days (10:00 LST)
CO2M[13]	global	2x2 km^2	planned for 2025	11 days (11:30 LST)
TEMPO/IS-40e[10]	18°N–58°N, 67°W–125°W	2.21 x 4.97 km^2	launched on Apr 7, 2023	geostationary (hourly)
Sentinel-4/MTG[12]	30°N–65°N, 30°W–45°E	8x8 km^2	planned for 2024	geostationary (hourly)

This table compares the coverage and resolution of the measurements in space, and time. The common names of SIF products are bolded, which will be referred to hereinafter

[1]SCIAMACHY: SCanning Imaging Absorption spectroMeter for Atmospheric CartograpHY; Envisat: Environment satellite; [101, 128]

[2]GOME: Global Ozone Monitoring Experiment; ERS-2: European Remote-Sensing 2; [99]

[3]GOME-2: Global Ozone Monitoring Experiment-2; MetOp-A: Meteorological Operational Satellites - A; [101]

[4]TANSO-FTS: Thermal And Near-infrared Spectrometer for carbon Observation-Fourier Transform Spectrometer; GOSAT: Greenhouse gases Observing SATellite; [129]

[5]TANSO-FTS: Thermal And Near-infrared Spectrometer for carbon Observation-Fourier Transform Spectrometer; GOSAT-2: Greenhouse gases Observing SATellite; [130]

[6]AGCS: Atmospheric Carbon dioxide Grating Spectroradiometer; TanSat: Carbon Dioxide Observation Satellite Mission; [103]

[7]OCO-2: Orbiting Carbon Observatory-2; [131]

[9]TROPOMI: TROPOspheric Monitoring Instrument; Sentinel-5p: Sentinel 5 Precursor; [82, 132]

[11]FLORIS: Fluorescence Imaging Spectrometer; FLEX: FLuorescence EXplorer; [110, 111]

[10]TEMPO: Tropospheric Emissions: Monitoring Pollution; IS-40e: Intelsat 40e; [133]

[12]MTG: Meteosat Third Generation; [134, 135]

[13]CO_2-M: the Copernicus CO_2 Monitoring satellite; [136]

noting that SIF measurements from a smaller footprint are more likely to be influenced by topography and thus need more rigorous corrections when instantaneous SIF measurements (Eq. 2) are normalized to daily mean values [65].

To provide more surface details at smaller spatial scales than the existing spaceborne measurements, there are several hybrid products that downscale SIF measurements to scales as fine as hundreds of meters using optical reflectance measurements and environmental data [112–117]. However, the accuracy of these downscaled global products (such as spatially contiguous SIF (CSIF) [113] and Global 'OCO-2' SIF (GOSIF) [114]) and their performance of tracking GPP have not been assessed across the Arctic-Boreal region at the finer spatial scale. Madani et al. [118] only validated the temporal variations of CSIF but not its spatial representativeness for a few Arctic-Boreal EC towers. Wen et al. [119] cross-validated the global spatial patterns of downscaled and satellite SIF products and found that downscaled SIF products can yield large biases in the Arctic-Boreal region because of the poor performance of universal downscaling models in this region. The higher noise in optical reflectance measurements due to background soil, water, and snow [66, 86, 113] can potentially affect the accuracy and reliability of the downscaled SIF products as well. To better train the downscaling models, more satellite observations with finer spatial resolutions in the Arctic-Boreal region are needed. Airborne instruments with much higher spatial resolutions (e.g., 30 m; Section 2.2) can help validate the spatial representativeness of downscaled products. However, such validation has only been done outside the Arctic-Boreal region [119]. Therefore, further validation and assessments of these downscaled products are needed for the Arctic-Boreal region to ensure their performance in this unique region.

Sampling Frequency and Overpass Time

The revisit time and swath width of satellites together determine the time required to complete one cycle of global SIF measurements and, thus, the sampling frequency at a

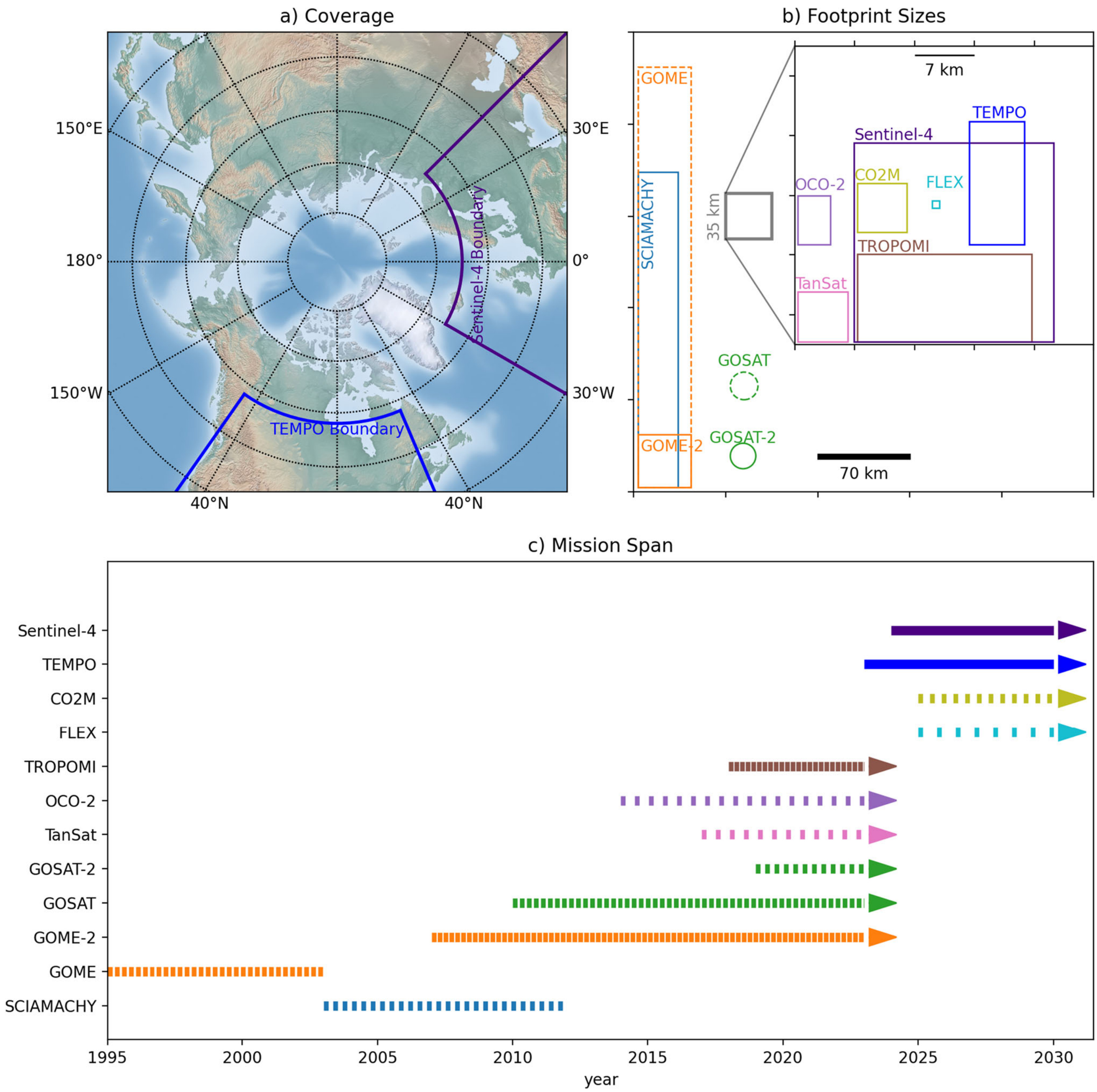

Fig. 2 A graphic summary of existing and upcoming satellite missions measuring SIF in the Arctic-Boreal region (north of 50°N): (a) The spatial coverage of satellites that do not cover the entire Arctic-Boreal region; (b) The comparison of satellite footprints; And (c) the mission span and temporal resolution of SIF measurements. In (c), arrows indicate ongoing or future missions, and dashes suggest the temporal resolution of SIF measurements. A densely dashed line means a higher temporal frequency. The exact value of temporal frequency can be referred to Table 1

specific location. These factors together determine the temporal coverage and resolution of SIF measurements in the Arctic-Boreal region. Existing and upcoming satellite missions have a wide range of sampling frequencies (Table 1, Fig. 2c), allowing for tracking the dynamics of SIF across temporal scales.

At seasonal and longer scales, polar-orbiting satellites have difficulties getting the complete and accurate seasonal cycle of SIF in the Arctic-Boreal region because of the lack of valid sampling during shoulder seasons and winters. Because SIF is driven by solar radiation (Eq. 2), to keep the measurement noises low, SIF measurements are often filtered out if they are taken at low solar radiation conditions, such as when the solar zenith angle exceeds certain thresholds. This will remove most of the observations during the Arctic-Boreal winters and potentially miss the onset and cessation of growing seasons depending on the threshold and sampling frequency (Fig. 3). A stricter threshold, such as 70° used in [82, 99], will exclude more SIF measurements during shoulder seasons compared to a looser threshold, such as 80° used in [109] (Fig. 3). This artificial cutoff of growing season varies by instruments with different sampling frequencies leading to misshaped growth seasonality, particularly for instruments with low sampling frequency [120, 121]. Missing the onset and cessation of GPP can cause large uncertainties in the net carbon flux during the shoulder seasons, when the majority of net carbon emission happens in the Arctic-Boreal region [122]. Such artificial cutoffs of growing season also fail to precisely track the temporal shifts of growth onset and cessation with climate change [33, 123, 124].

To track the subdaily and diurnal variations of photosynthesis, satellite missions/instruments like TROPOMI with different overpass times at certain locations can be useful [125, 126]. Additionally, geostationary satellite missions/instruments like TEMPO, Sentinel-4, and canceled Geostationary Carbon Cycle Observatory (GeoCarb) [127] can offer multiple SIF measurements each day. Unfortunately, none of the existing or upcoming geostationary satellite missions have complete coverage in space for the Arctic-Boreal region (Table 1, Fig. 2a). Therefore, relying on satellite SIF measurements alone is challenging to track the subdaily and diurnal variations in photosynthesis in the entire Arctic-Boreal region. Instead, tower-based instruments can be more feasible for tracking the dynamics of SIF at a sub-daily scale and over longer terms (Section 2.3).

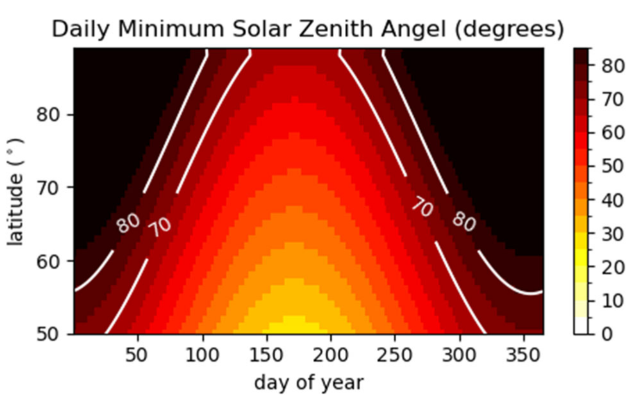

Fig. 3 The zonal mean of minimum solar zenith angle over a year, representing the availability of solar radiation at the local solar noon across different latitudes. The minimum solar zenith angle greater than 90° means polar night, when solar radiation is zero throughout the day. The white contours represent the two common thresholds for filtering out SIF measurements at low solar radiation conditions (80° in [109] and 70° in [82, 99])). These thresholds indicate the maximum solar zenith angle (minimum solar radiation) acceptable for valid SIF measurements. SIF measurements taken at solar zenith angles higher than the thresholds are excluded due to the low signal-to-noise ratio

Airborne SIF

As an analog of spaceborne instruments, airborne instruments measure SIF at enhanced spatial resolutions benefiting from a closer distance between the aircraft and the ground. Among a few airborne SIF instruments (summarized in [137]), NASA Jet Propulsion Laboratory's Chlorophyll Fluorescence Imaging Spectrometer (CFIS) [138] is the only instrument has extensively flown in the Arctic-Boreal region. During NASA's Arctic-Boreal Vulnerability Experiment (ABoVE) airborne campaign in 2017 [139], CFIS SIF was retrieved at the finest resolution of 30 m, with a focus on more than 20 EC tower sites across Alaska and northwest Canada [140]. Unfortunately, there has not been reported SIF-GPP relationship using CFIS SIF. Tagliabue et al. [95] reported r^2 of 0.5 between the snapshots of GPP and SIF from a European airborne instrument (HyPlant). The optimal airborne SIF-GPP relationship can be achieved by spatially aggregating SIF observations (Fig. 1). Therefore, the small pixels of CFIS SIF, together with optical reflectance measurements, can better resolve the spatial distribution of different land covers [91, 102, 141] and align with the footprints of EC GPP [142, 143]. The existing collections of snapshots can also help validate the spatial representativeness of downscaled SIF products discussed in Section 2.1.1. However, such validation with a few snapshots does not hold over time. For example, CFIS sampled SIF in the Arctic-Boreal region for only two days during the ABoVE airborne campaign in 2017. Without additional repeated sampling, it is challenging to assess the rapid and heterogeneous changes of Arctic-Boreal vegetation under climate change.

Tower-Based SIF

Existing tower-based instruments (summarized in [98]) are competent for continuously measuring day-to-day and subdaily variations in SIF at specific locations. Tower-based SIF and EC GPP measurements often have overlapping footprints [57], making them ideal for deriving SIF-GPP relationships at diurnal and seasonal scales [66, 144].

However, similar to the spatially limited EC GPP measurements, tower-based SIF measurements are also scarce in the Arctic-Boreal region. Currently, PhotoSpec (in Delta Junction, Alaska and in Saskatchewan, Canada) [96] and FluoSpec2 (in Toolik, Alaska) [145] are the only tower-based instruments actively measuring SIF in the Arctic-Boreal region, which hinders extensive examination of SIF-GPP relationship across the Arctic-Boreal region. Only two Boreal forests have reported tower-based SIF-GPP relationship (Fig. 1; [66, 96, 97]). Nevertheless, novel tower-based SIF observation systems are progressing quickly with the potential to be deployed in the Arctic-Boreal region, e.g., Tower Spectrometer on Wheels for Investigating Frequent Timeseries (TSWIFT; [146]), the Fluorescence Box (JB Hyperspectral; Dusseldorf, Germany), Automatically long-term SIF observation system (AutoSIF; [83]), the Fluorescence Auto-Measurement Equipment (FAME; [147]), and a NASA/Goddard Space Flight Center Prototype for Field Spectroscopy (FUSION). The specifications of these tower-based SIF observation systems are summarized in Table 2. It is worth noting that these systems have various spectral characteristics, field of view, and mobility (Table 2), which are critical for the representativeness of SIF retrievals and comparison retrievals across different systems. For example, although tower-based SIF is often retrieved at around 760 nm, the various spectral ranges and spectral resolutions (Full Width at Half Maximum) lead to uncertainties in the retrieved SIF values [99, 148]. The accuracy of different retrieval algorithms is summarized by Mohammed et al. [92].

A small field of view, such as in PhotoSpec, makes it easy to target individual trees, filter out background noises (e.g., snow), and resolve SIF signals from different parts of the canopy by scanning individual trees [149]. Pierrat et al. [96] remotely detected diverse growing onsets across species in a mixed-species Boreal forest by taking advantage of the small field of view in PhotoSpec.

The directional effect between the solar incidence angle and the viewing angle is not negligible for tower-based instruments because of large variations in the solar incidence angle in the Arctic-Boreal region [150]. The directional effect can be reduced by fusing observations from different view geometries [146, 151]. Therefore, the systems with scanning telescopes, e.g., PhotoSpec, TSWIFT, and FUSION, are advantageous, although harsh winter weather can be challenging for the parts of rotating mechanics.

Enhancing Cross-scale Observational Network

Airborne and tower-based SIF measurements complement the coarse spatiotemporal resolutions of spaceborne SIF in the Arctic-Boreal region. However, the current availability of airborne and tower-based instruments is constrained to a few sites and a brief sampling duration in the Arctic-Boreal region compared to lower latitudes. Additionally, regional studies on the Arctic-Boreal vegetation dynamics are imbalanced across continents, with a greater focus on North America than Eurasia as a result of imbalanced data availability, while Eurasia is also a significant contributor to the global carbon cycle [124]. Therefore, enhancing the international network of airborne and tower-based SIF measurements is the key to validating spaceborne measurements and investigating scale-dependent vegetation dynamics throughout the entire Arctic-Boreal region [91, 107].

As sensing technology advances, flying lower-cost and lighter airborne instruments on Unmanned Aerial Vehicles (UAV) becomes convenient to provide frequent SIF measurements at fine spatial resolution [152, 153]. More encouragingly, collaborations among agencies are exploring the opportunities to fly airborne instruments more frequently and regularly, such as NASA ABoVE and National Ecological Observatory Network (NEON) airborne observation platform [139].

Table 2 Existing and new SIF observation systems

Systems	Spectral Range (nm) (FWHM[1] (nm))	Field of View	Mobility	Examples in the Arctic-Boreal region
PhotoSpec[2]	650–712 (0.3), 729–784 (0.3)	0.7°	2-D scanning	[96, 144]
FluoSpec2[3]	730–780 (0.14)	25	Downward looking	[145]
TSWIFT[4]	729–784 (0.3)	0.7	2-D scanning and mobile	–
FLOX[5]	650–800 (0.3)	25	Downward looking	–
AutoSIF[6]	640–805 (0.3)	25	Downward looking	–
FAME[7]	730–786 (0.15)	25	Downward looking	–
FUSION[8]	650–840 (1.5)	25	2-D scanning	–

This table compares the spectral characteristics, field of view, and mobility of these systems
[1]FWHM: Full Width at Half Maximum;
[2]PhotoSpec [149]
[3]FluoSpec2 [145]
[4]TSWIFT: Tower Spectrometer on Wheels for Investigating Frequent Timeseries; [146]
[5]FLOX: the Fluorescence Box; JB Hyperspectral, Dusseldorf, Germany;
[6]AutoSIF: Automatically long-term SIF observation system; [83]
[7]FAME: the Fluorescence Auto-Measurement Equipment; [147]
[8]FUSION: a NASA/Goddard Space Flight Center Prototype for Field Spectroscopy;

The success of volunteer-based EC networks, such as Fluxnet, is an excellent example of strengthening carbon cycle studies through global collaboration [57]. In the spectral imaging community, a similar network of optical reflectance called SpecNet [154] has made fruitful findings to boost the connections between remote sensing and carbon uptake [155]. There are only a few tower-based SIF measurements in the Arctic-Boreal region and mostly in North America. Going forward, fostering a similar tower-based SIF network is strongly favored for understanding the biochemical and biophysical processes in the Arctic-Boreal region. The two PhotoSpec instruments [96, 144] and one FluoSpec2 instrument [145] are prototypes of such a network, showing promise in this regard. Expanding the SIF network in the Arctic-Boreal region is viable with lower-cost and easier-maintained sensors [156, 157].

Quantitative Estimation of GPP in the Arctic-Boreal Region

Empirical SIF-GPP Relationship

GPP is often quantitatively evaluated by satellite SIF using empirical models at the seasonal scale [66, 158]. Taking Eqs. (1) and (2) together, inferring seasonal GPP from $\mathrm{SIF_{dc}}$ leads to solving the GPP/$\mathrm{SIF_{dc}}$ ratio (k), which contains the information of LUE, Φ_F, and f_{esc}:

$$\mathrm{GPP} = \mathrm{k} \times \mathrm{SIF_{dc}}, \tag{3}$$

$$\mathrm{k} = f(LUE, \Phi_F, f_{\mathrm{esc}}). \tag{4}$$

At the canopy level, this SIF-GPP relationship (Eq. 3) is approximately linear such that k is relatively constant across different months [159, 160]. Empirical studies [66, 161–163] solve the parameter k by linearly regressing GPP and SIF. Then, the k values are categorized based on generic plant functional type to integrally represent different plant physiology (e.g., LUE and Φ_F) and canopy structures (e.g., f_{esc}) (Eq. 4). The first study [66] to derive k values for unique Arctic-Boreal land cover types shows that high-stature land cover types (e.g., evergreen and deciduous forests) have higher k than lower-stature land cover types (e.g., low shrubs and tundra). However, the reported k values still have large uncertainties inherited from SIF and GPP datasets due to large footprints, background noise, and lack of validation [90, 164]. Validating the satellite SIF and GPP measurements with more evenly distributed tower-based SIF and GPP can significantly reduce extrapolation [165] and improve the confidence of k values and GPP predictions thanks to relatively small and homogeneous footprints of tower-based instruments [66, 166, 167]. The spatial representativeness of k values within the footprint of tower-based instruments can be further validated with airborne snapshots [91] once more repeated airborne missions are available.

As the record of SIF measurements becomes longer, mapping the changes in GPP over the long term is possible. In the Arctic-Boreal region, the empirically derived k should be calibrated regularly to keep up to date with the changing plant composition and canopy structure due to warming, such as shrub expansion, forest-tundra ecotone shifts, and wildfires. Within a satellite footprint, these changes can be reflected in the mixing of vegetation types and changes in k. However, there are not sufficient observations to quantify such changes [168] including SIF.

There have been discussions on the goodness of assuming linear SIF-GPP relationship [162, 167]. Interestingly, the reported SIF-GPP relationship in the Arctic-Boreal region is debatable. At monthly and daily scales, the Arctic-Boreal k value of the linear SIF-GPP relationship shifts with season (Fig. 4a) according to both regional-scale [66, 118, 167] and tower-based [144] studies. As the temporal scale refines to half-hourly, the SIF-GPP relationship becomes nonlinear (Fig. 4b) due to small light response of SIF in winter and seasonal variations in light use efficiency [144]. There have not been mechanistic analyses exploring the linearity/nonlinearity of SIF-GPP relationship over the entire Arctic-Boreal region. Existing global-scale analyses attribute the nonlinearity to the nonlinear response to environmental stresses [166, 169] and aggregated directional effect [80, 170, 171]. Considering environmental stresses caused by climate change, large seasonal variations of solar incidence angle, and heterogeneous canopy structure in the Arctic-Boreal region, more work should be done to mechanistically explain the linearity/nonlinearity of the SIF-GPP relationship across this region. Future works resolving such complex roles of climate drivers and radiative factors on the SIF-GPP relationship will also benefit from evaluating the climate change impacts on carbon uptake and tracking physiological and structural changes of Arctic-Boreal vegetation at different temporal scales.

Machine Learning Models

Without the need to solve the complex mechanisms, machine learning approaches [166, 172, 173] conveniently offer a potential solution to simulate the complex SIF-GPP relationship and predict GPP using satellite SIF, optical reflectance, environmental data, and land cover information. FluxSat and FluxSat V2.0 are examples of such datasets [172, 174, 175]. In FluxSat, the prediction of GPP in high productivity areas directly benefits from incorporating SIF [174]. In other regions, including the Arctic-Boreal region, the significance of SIF data for the machine learning-based GPP prediction needs further investigations [172]. Meanwhile, these machine learning models also inherent the compounded

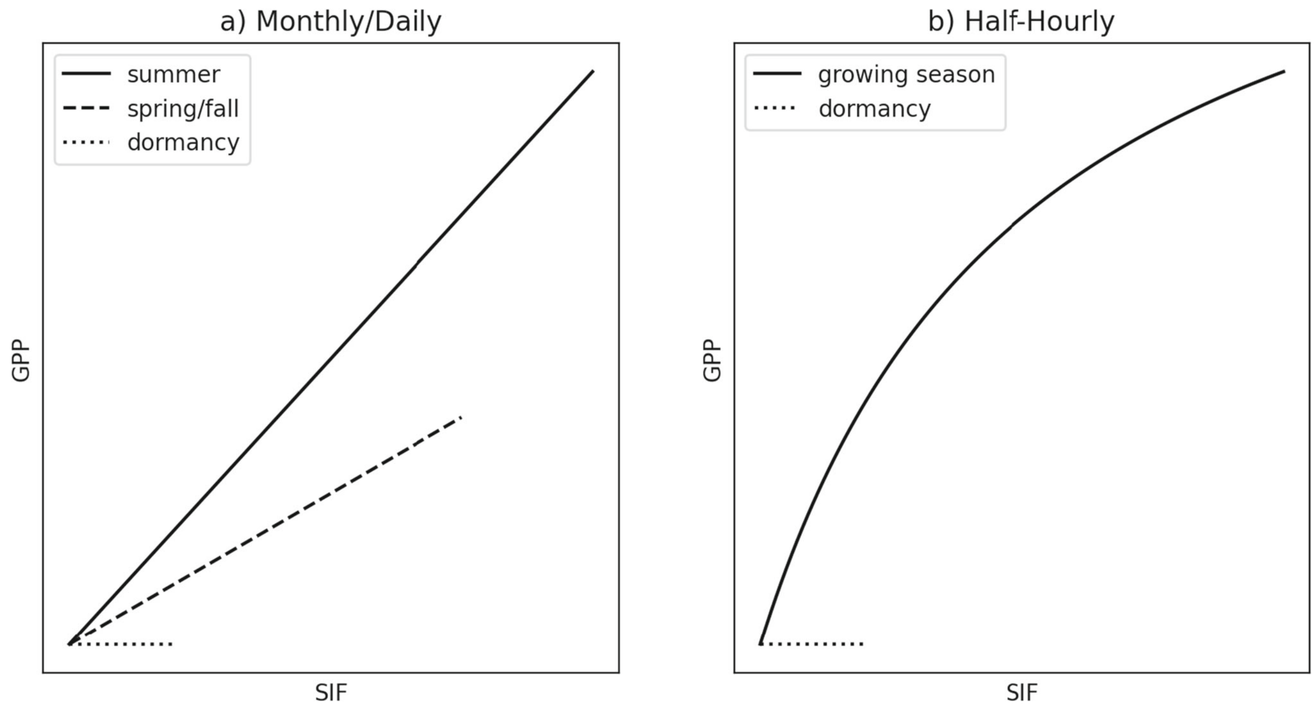

Fig. 4 A graphic demonstration of the seasonal variations in (a) linear and (b) nonlinear SIF-GPP relationships reported by Pierrat et al. [144] and Chen et al. [167]. The linear relationship is mostly found in monthly or daily scale analyses. The nonlinear relationship is mostly found in half-hourly scale analyses. The linear relationship follows Eq. 3. The nonlinear relationship follows the mathematical form of $y = a * x/(b + x)$ [144]. Dormancy has a smaller range of SIF due to the low productivity in the Arctic-Boreal region. Outside the dormancy, there is not enough evidence to determine the relative magnitudes of the nonlinear relationship curve from season to season

uncertainties from SIF and other optical remote sensing observations in the Arctic-Boreal region, such as spatial heterogeneity (Section 2.1) and snow contamination [66]. More tower-based observations of both GPP and SIF across the Arctic-Boreal region can help reduce the extrapolation uncertainties [165] and improve the accuracy of machine learning models in the Arctic-Boreal region.

Advances in Carbon Cycle Modeling with SIF

Intrinsically, process-based models (Table 3) simulate GPP using parameterized photosynthetic traits, e.g., the maximum rate of carboxylation and photosynthesis yield, [176]. These parameters are estimated based on tower-based measurements and then extrapolated globally [177].

Dynamic vegetation models and [123, 178, 179] and other process-based terrestrial ecosystem models [180–182] simulate the mechanics of fluorescence and radiative transfer, where SIF measurements can be assimilated into these models and optimize the photosynthetic parameters. On the other hand, conventional land surface models, which do not simulate SIF directly, SIF-driven GPP can be used to optimize the parameterized photosynthetic traits and constrain the errors in simulating global carbon fluxes in land surface models [183–186]. In the Arctic-Boreal region, GPP simulated by the optimized models has improved the spatial distribution and temporal patterns, which reveal a strong reduction of GPP in the Arctic-Boreal region [123, 178, 187].

Recently, there has been significant progress in simulating radiative transfer and SIF within land surface models [188]. This advancement provides opportunities for physically simulating the SIF-GPP relationship. Future studies can benchmark the model simulation with remote sensing in order to better map photosynthetic traits and investigate the complex climate drivers of carbon fluxes, especially in the Arctic-Boreal region.

One drawback of these models is their global universal parameterization, which often neglects or oversimplifies the complex vegetation distribution and land cover types in the Arctic-Boreal region, leading to large uncertainties in the simulated carbon fluxes and their spatial variations. Better resolving the SIF-GPP relationship for Arctic-Boreal land cover types [118] and justifying its spatial representativeness given the heterogeneous land cover within coarse footprints [91, 168] is critical for simulating spatially detailed changes in carbon fluxes.

Table 3 Process-based models that incorporate SIF

Type	Models
Dynamic vegetation models	TRENDY [123]; Terrestrial Biosphere Model (TBM [178]; Lund-Potsdam-Jena managed Land (LPJmL4) [179]
Other process-based terrestrial ecosystem models	Boreal Ecosystem Productivity Simulator (BEPS) [180]; Biosphere Energy Transfer Hydrology-Soil Canopy Observation, Photosynthesis and Energy fluxes (BETHY-SCOPE); [181]; Mechanistic Light Reaction-SIF model (MLR-SIF) [182]
Land surface models	Energy Exascale Earth System Model (E3SM) [183]; Community Land Model version 4.5 (CLM4.5) [184]; Community Land Model version 5 (CLM5 [185]); JSBACH [186]

Emergent Changes in Arctic-Boreal Region

As SIF measurements become more abundant in the Arctic-Boreal region, we are gaining more insights into mechanistically tracking GPP using SIF data obtained at various spatiotemporal scales [189]. This section focuses on reviewing the applications of SIF in monitoring crucial changes in the Arctic-Boreal region [10]. Meanwhile, outlooks on future research are provided for deepening our understanding of the resulting changes in the global carbon cycle.

Arctic "Greening"/"Browning" and Its Climate Drivers

Under the scenario of global warming, Arctic "greening" and "browning" have been signature indicators of changing vegetation dynamics, which are composed of changes in vegetation phenology and vegetation distribution [32]. SIF has been mostly used in evaluating the vegetation phenology over the Arctic-Boreal region, including the peak GPP during the growing season, the timing of growth onset and cessation, and the length of the growing season. Implementing SIF in detecting changes in vegetation distribution and land cover types is understudied.

Vegetation Phenology

Large-scale and long-term studies [32, 190–192] rely on long records of satellite greenness measurements, such as NDVI or EVI, to evaluate changes in vegetation phenology across the Arctic-Boreal region. However, these greenness measurements primarily reflect APAR and leaf area rather than actual GPP [71, 72]. This limitation restricts the accurate estimation of changing carbon fluxes and the identification of underlying mechanisms driving these changes [193–195], especially in needle-leaf forests where the responses of GPP and greenness measurements to climate diverge [86, 89, 196]. Since SIF varies with both APAR and LUE, it is a better proxy than the greenness measurements for tracking the seasonal GPP across various land cover types in the Arctic-Boreal region [85, 88, 197].

The spring onsets of SIF and GPP in the Arctic-Boreal region closely follow the rising temperature and landscape thawing [86, 194, 198, 199], which is consistent with findings from proximal measurements in a sub-alpine ecosystem [200]. Warming causes extended non-frozen periods, leading to a longer growing season [33, 201]. Both SIF and GPP indicate that an early onset caused by warming may induce reduced magnitude of photosynthesis in fall, as soil moisture depletes [202]. Meanwhile, exposure to cold temperatures can delay the spring onset of SIF and GPP [203]. It is worth noting that the onset of SIF may occur earlier than GPP due to the earlier activation of the photosystem compared to photosynthesis [204].

The cessation of SIF and GPP in the Arctic-Boreal region is regulated by temperature, soil moisture, and radiation [193, 205–208]. In ecosystems with weaker radiation limitation, GPP increases more with warming compared to the ecosystems strongly limited by radiation [209]. SIF and GPP have an earlier cessation than canopy greenness due to divergent responses to temperature in the fall [89]. As the Arctic-Boreal region warms, the cessation of growth is projected to be more water-limited [33, 194, 205].

In the long term, the existing satellite SIF measurements do not have sufficiently long records to robustly derive the trends in changing vegetation phenology (Fig. 2c) compared to conventional greenness measurements (e.g., more than 50-year records of Landsat reflectance [210]). Nevertheless, SIF records have been mostly used to validate the long-term trend observed from the vegetation indices of greenness measurements. SIF measurements in the Arctic-Boreal region agree with greenness measurements in showing that warming leads to an earlier and higher peak in GPP [118, 201, 211–213]. However, further warming will not continue promoting GPP once the optimal temperature is surpassed [214, 215]. Notably, the peaks of GPP and SIF occur earlier than the peak of greenness, indicating a decoupling of peak timing between photosynthetic rate and canopy greenness [90]. This mismatch between the peaks, which could be a result of delayed canopy development, increases with rising atmospheric CO^2 and reduced maximum photosynthetic rate [216].

Across the Arctic-Boreal region, these temporal changes in vegetation phenology are not homogeneous [32]. Madani et al. [118] use CSIF, a downscaled SIF product, to study the spatial pattern of changes in Arctic-Boreal phenology and suggest that such heterogeneous climate sensitivity can be explained at the regional level and characterized by plant functional traits. Incorporating SIF with better-represented plant functional traits in land surface models can improve the estimation of carbon fluxes as vegetation phenology changes.

Detecting Land Cover Changes and Vegetation Compositions

So far, this paper has mainly focused on far-red SIF. However, it is important to note that SIF emissions include both red and far-red wavelengths. Remote sensing instruments often report canopy-scale SIF in far-red wavelengths because of the reabsorption of red SIF by chlorophyll [217]. The ratio between red and far-red SIF at the leaf level can provide additional information about biochemical traits, leaf morphology, and photosynthetic phenology [218, 219]. Therefore, the leaf-level red:far-red SIF ratio may help to identify plant functional type and monitor land cover changes [220]. However, this conclusion may not hold at the canopy level with remotely measured SIF due to the reabsorption of red SIF.

Droughts and Wildfires

Rapid warming in the Arctic-Boreal region is projected to increase the frequency of droughts and wildfires, which may interrupt the increasing trend of GPP and release CO^2 from thawing permafrost into the atmosphere. SIF measurements have been used to monitor ecosystem response to these disturbances and recovery.

Droughts

A case study of the 2010 Russian drought [221] uses SIF and greenness measurements to show that the drought impact on GPP through both reduced fPAR and LUE (refer to Eqs. 1 and 2). However, the reduction of LUE dominates the decreasing GPP in forests, while the reduction of fPAR is the main reason for the decreasing GPP in grasslands. Furthermore, Li et al. [222] use SIF as a proxy for photosynthetic phenology and find that Arctic-Boreal forests recovery from droughts not only depends on the severity of droughts but also the relative timing of droughts and vegetation phenology.

More advanced, SIF can help understand the ecosystem response to droughts from an ecohydrology perspective as transpiration and photosynthesis are coupled processes. For example, Recent studies [206, 223–225] use SIF to mechanistically constrain the dynamics of transpiration and characterize the seasonal patterns of transpiration in the Arctic-Boreal region, suggesting SIF has the potential to investigate climate drivers of carbon and water cycles simultaneously.

The diurnal dynamics of photosynthesis are important for understanding the coupled carbon-water cycles and ecosystem-climate feedbacks [226]. In the Arctic-Boreal region, the diurnal variations of GPP characterized by tower-based measurements reveal a nonlinear relationship between SIF-GPP in Boreal forests due to light saturation [144], underlying significance of the diurnal SIF measurements for improving the modeling of the vegetation dynamics. Spaceborne instruments, such as TROPOMI, TEMPO, and Sentinel-4, provide great potential for measuring SIF at different times of the day, while TROPOMI is the only instrument that covers the entire Arctic-Boreal region. The diurnal pattern of TROPOMI SIF is consistent with GPP [126] indicating the potential of evaluating diurnal variations of carbon-water cycles from space [227].

To comprehensively characterize biochemical and biophysical processes, combining multi-modal remote sensors (including SIF instruments) and addressing different components of the carbon-water cycles are beneficial. For example, using visible-near infrared reflectance (including SIF), microwave, lidar, and thermal imaging to simultaneously monitor photosynthesis, ecohydrology, canopy structure, and water stress in respective. For future reference in the Arctic-Boreal region, applying this multi-modal concept is available from space [228–230], aircraft [231], and towers [232].

Wildfires

In the case of wildfires, applying SIF to monitoring the change in GPP can be challenging because the SIF-GPP relationship may change if wildfires alter the plant composition as discussed in Section 3.1. Madani et al. [213] compare burned and unburned areas with the same land cover types and show that SIF-driven GPP has shown a faster recovery after wildfires happened, although there is an instantaneous decrease in GPP during wildfires [213].

Conclusion and Future Directions

This paper comprehensively summarizes cross-scale SIF instruments and new insights gained regarding carbon fluxes by using SIF in the Arctic-Boreal region. Through a thorough review of existing and upcoming satellite missions/instruments, this paper highlights the complementary nature of spaceborne, airborne, and tower-based SIF measurements, which collectively enable wide-ranging spatiotemporal coverage and resolutions in the Arctic-Boreal region. These cross-scale SIF measurements provide new insights into long-term variations and spatial patterns of photosynthetic dynamics and the carbon uptake from subdaily to seasonal scales in the Arctic-Boreal region, which are key to mechanistically constraining the carbon fluxes in land surface models.

For future references, it is important to acknowledge that current SIF measurements in the Arctic-Boreal region are still limited and their spatial resolutions are too coarse for the heterogeneous land cover. Overcoming these limitations requires fostering an extensive SIF observational network to improve land surface modeling in the Arctic-Boreal region and validate existing quantitative models. Integration of multi-modal instruments that combine SIF and other (a)biotic variables holds promise to comprehensively represent the diverse plant functional traits and their climate sensitivity with climate change. Such data synergies and model improvements are becoming possible as both NASA ABoVE and the Department of Energy's Next Generation Ecological Experiment in the Arctic (DOE NGEE-Arctic) are towards their ending phases, which focus on data synthesis and modeling. Taken together, SIF still has great potential for advancing our understanding of the ecosystem-climate feedbacks and projecting climate change impact across the Arctic-Boreal region.

Acknowledgements I would like to acknowledge anonymous reviewers for their constructive feedback and insightful comments. This review would not be finished without their valuable contributions.

Author Contributions Rui Cheng finished the entire manuscript.

Funding 'Open Access funding provided by the MIT Libraries'. This work was supported by the National Science Foundation Disrupting Operations of Illicit Supply Networks under Grant No. 2039771.

Data Availability No new data is generated with this article. All data used in this article are cited with their publication DOIs.

Declarations

Conflict of Interest The authors declare no competing interests.

References

1. Pan Y, Birdsey RA, Fang J, Houghton R, Kauppi PE, Kurz WA, et al. A large and persistent carbon sink in the world's forests. Science. 2011;333(6045):988–93. https://doi.org/10.1126/science.1201609.
2. Virkkala AM, Aalto J, Rogers BM, Tagesson T, Treat CC, Natali SM, et al. Statistical upscaling of ecosystem CO_2 fluxes across the terrestrial tundra and boreal domain: regional patterns and uncertainties. Glob Change Biol. 2021;27(17):4040–59. https://doi.org/10.1111/gcb.15659.
3. Eyring V, Bony S, Meehl GA, Senior CA, Stevens B, Stouffer RJ, et al. Overview of the coupled model intercomparison project Phase 6 (CMIP6) experimental design and organization. Geosci Model Dev. 2016;9(5):1937–58. https://doi.org/10.5194/gmd-9-1937-2016.
4. Braghiere RK, Fisher JB, Miner KR, Miller CE, Worden JR, Schimel DS, et al. Tipping point in North American Arctic-Boreal carbon sink persists in new generation Earth system models despite reduced uncertainty. Environ Res Lett. 2023;18(2):025008. https://doi.org/10.1088/1748-9326/acb226.
5. Watts JD, Farina M, Kimball JS, Schiferl LD, Liu Z, Arndt KA, et al. Carbon uptake in Eurasian boreal forests dominates the high-latitude net ecosystem carbon budget. Glob Change Biol. 2023;29(7):1870–89. https://doi.org/10.1111/gcb.16553.
6. Rantanen M, Karpechko AY, Lipponen A, Nordling K, Hyvärinen O, Ruosteenoja K, et al. The Arctic has warmed nearly four times faster than the globe since 1979. Commun Earth Environ. 2022;3(1):168. https://doi.org/10.1038/s43247-022-00498-3.
7. Schuur EAG, Vogel JG, Crummer KG, Lee H, Sickman JO, Osterkamp TE. The effect of permafrost thaw on old carbon release and net carbon exchange from tundra. Nature. 2009;459(7246):556–9. https://doi.org/10.1038/nature08031.
8. Natali SM, Schuur EAG, Rubin RL. Increased plant productivity in Alaskan tundra as a result of experimental warming of soil and permafrost. J Ecol. 2012;100(2):488–98. https://doi.org/10.1111/j.1365-2745.2011.01925.x.
9. Natali SM, Schuur EAG, Webb EE, Pries CEH, Crummer KG. Permafrost degradation stimulates carbon loss from experimentally warmed tundra. Ecology. 2014;95(3):602–8. https://doi.org/10.1890/13-0602.1.
10. Box JE, Colgan WT, Christensen TR, Schmidt NM, Lund M, Parmentier FJW, et al. Key indicators of Arctic climate change: 1971–2017. Environ Res Lett. 2019;14(4):045010. https://doi.org/10.1088/1748-9326/aafc1b.
11. Chen Y, Romps DM, Seeley JT, Veraverbeke S, Riley WJ, Mekonnen ZA, et al. Future increases in Arctic lightning and fire risk for permafrost carbon. Nat Clim Change. 2021;11(5):404–10. https://doi.org/10.1038/s41558-021-01011-y.
12. Descals A, Gaveau DLA, Verger A, Sheil D, Naito D, Peñuelas J. Unprecedented fire activity above the Arctic Circle linked to rising temperatures. Science. 2022;378(6619):532–7. https://doi.org/10.1126/science.abn9768.
13. Mack MC, Bret-Harte MS, Hollingsworth TN, Jandt RR, Schuur EAG, Shaver GR, et al. Carbon loss from an unprecedented Arctic tundra wildfire. Nature. 2011;475(7357):489–92. https://doi.org/10.1038/nature10283.
14. McCarty JL, Aalto J, Paunu VV, Arnold SR, Eckhardt S, Klimont Z, et al. Reviews and syntheses: arctic fire regimes and emissions in the 21st century. Biogeosciences. 2021;18(18):5053–83. https://doi.org/10.5194/bg-18-5053-2021.
15. Tape K, Sturm M, Racine C. The evidence for shrub expansion in Northern Alaska and the Pan-Arctic: Shrub Expansion in Northern Alaska and Pan-Arctic. Glob Change Biol. 2006;12(4):686–702. https://doi.org/10.1111/j.1365-2486.2006.01128.x.

16. Pearson RG, Phillips SJ, Loranty MM, Beck PSA, Damoulas T, Knight SJ, et al. Shifts in Arctic vegetation and associated feedbacks under climate change. Nat Clim Change. 2013;3(7):673–7. https://doi.org/10.1038/nclimate1858.
17. Orndahl KM, Macander MJ, Berner LT, Goetz SJ. Plant functional type aboveground biomass change within Alaska and northwest Canada mapped using a 35-year satellite time series from 1985 to 2020. Environ Res Lett. 2022;17(11):115010. https://doi.org/10.1088/1748-9326/ac9d50.
18. Angert A, Biraud S, Bonfils C, Henning CC, Buermann W, Pinzon J, et al. Drier summers cancel out the CO_2 uptake enhancement induced by warmer springs. Proc Natl Acad Sci. 2005;102(31):10823–7. https://doi.org/10.1073/pnas.0501647102.
19. Zona D, Lafleur PM, Hufkens K, Bailey B, Gioli B, Burba G, et al. Earlier snowmelt may lead to late season declines in plant productivity and carbon sequestration in Arctic tundra ecosystems. Sci Rep. 2022;12(1):3986. https://doi.org/10.1038/s41598-022-07561-1.
20. Piao S, Friedlingstein P, Ciais P, Viovy N, Demarty J. Growing season extension and its impact on terrestrial carbon cycle in the Northern Hemisphere over the past 2 decades: Phenology and Carbon Cycle in NH. Glob Biogeochem Cycles. 2007;21(3). https://doi.org/10.1029/2006GB002888.
21. Zhang Y, Piao S, Sun Y, Rogers BM, Li X, Lian X, et al. Future reversal of warming-enhanced vegetation productivity in the Northern Hemisphere. Nat Clim Change. 2022;12(6):581–6. https://doi.org/10.1038/s41558-022-01374-w.
22. Zona D, Lafleur PM, Hufkens K, Gioli B, Bailey B, Burba G, et al. Pan-Arctic soil moisture control on tundra carbon sequestration and plant productivity. Glob Change Biol. 2023;29(5):1267–81. https://doi.org/10.1111/gcb.16487.
23. Keeling CD, Chin JFS, Whorf TP. Increased activity of northern vegetation inferred from atmospheric CO2 measurements. Nature. 1996;382(6587):146–9. https://doi.org/10.1038/382146a0.
24. Walker XJ, Alexander HD, Berner LT, Boyd MA, Loranty MM, Natali SM, et al. Positive response of tree productivity to warming is reversed by increased tree density at the Arctic tundra–taiga ecotone. Can J For Res. 2021;51(9):1323–38. https://doi.org/10.1139/cjfr-2020-0466.
25. Barichivich J, Briffa KR, Myneni RB, Osborn TJ, Melvin TM, Ciais P, et al. Large-scale variations in the vegetation growing season and annual cycle of atmospheric CO_2 at high Northern latitudes from 1950 to 2011. Glob Change Biol. 2013;19(10):3167–83. https://doi.org/10.1111/gcb.12283.
26. Myneni RB, Keeling CD, Tucker CJ, Asrar G, Nemani RR. Increased plant growth in the Northern high latitudes from 1981 to 1991. Nature. 1997;386(6626):698–702. https://doi.org/10.1038/386698a0.
27. Schwartz MD, Ahas R, Aasa A. Onset of spring starting earlier across the Northern Hemisphere: onset of NH Spring Starting Earlier. Glob Change Biol. 2006;12(2):343–51. https://doi.org/10.1111/j.1365-2486.2005.01097.x.
28. Buermann W, Bikash P, Jung M, Burn DH, Reichstein M. Earlier springs decrease peak summer productivity in North American boreal forests. Environ Res Lett. 2013;8(2):024027. https://doi.org/10.1088/1748-9326/8/2/024027.
29. Piao S, Tan J, Chen A, Fu YH, Ciais P, Liu Q, et al. Leaf onset in the northern hemisphere triggered by daytime temperature. Nat Commun. 2015;6(1):6911. https://doi.org/10.1038/ncomms7911.
30. Liu Q, Fu Y, Zhu Z, Liu Y, Liu Z, Huang M, et al. Delayed autumn phenology in the Northern Hemisphere is related to change in both climate and spring phenology. Glob Change Biol. 2016;22(11):3702–11. https://doi.org/10.1111/gcb.13311.
31. Buermann W, Forkel M, O'Sullivan M, Sitch W, Friedlingstein P, Haverd V, et al. Widespread seasonal compensation effects of spring warming on northern plant productivity. Nature. 2018;562(7725):110–4. https://doi.org/10.1038/s41586-018-0555-7.
32. Myers-Smith IH, Kerby JT, Phoenix GK, Bjerke JW, Epstein HE, Assmann JJ, et al. Complexity revealed in the greening of the Arctic. Nat Clim Change. 2020;10(2):106–17. https://doi.org/10.1038/s41558-019-0688-1.
33. Kim Y, Kimball JS, Parazoo N, Kirchner P. Diagnosing environmental controls on vegetation greening and browning trends over Alaska and Northwest Canada using complementary satellite observations. In: Yang D, Kane DL, editors. Arctic Hydrology, Permafrost and Ecosystems. Cham: Springer International Publishing; 2021. pp 583–613. Available from: http://link.springer.com/10.1007/978-3-030-50930-9_20.
34. Friedlingstein P, O'Sullivan M, Jones MW, Andrew RM, Bakker DCE, Hauck J, et al. Global carbon budget 2023. Earth Syst Sci Data. 2023;15(12):5301–69. https://doi.org/10.5194/essd-15-5301-2023.
35. Fisher JB, Sikka M, Oechel WC, Huntzinger DN, Melton JR, Koven CD, et al. Carbon cycle uncertainty in the Alaskan Arctic. Biogeosciences. 2014;11(15):4271–88. https://doi.org/10.5194/bg-11-4271-2014.
36. McGuire AD, Anderson LG, Christensen TR, Dallimore S, Guo L, Hayes DJ, et al. Sensitivity of the carbon cycle in the Arctic to climate change. Ecol Monogr. 2009;79(4):523–55. https://doi.org/10.1890/08-2025.1.
37. Loisel J, Gallego-Sala AV, Amesbury MJ, Magnan G, Anshari G, Beilman DW, et al. Expert assessment of future vulnerability of the global peatland carbon sink. Nat Clim Change. 2021;11(1):70–7. https://doi.org/10.1038/s41558-020-00944-0.
38. Rogers A, Serbin SP, Way DA. Reducing model uncertainty of climate change impacts on high latitude carbon assimilation. Glob Change Biol. 2022;28(4):1222–47. https://doi.org/10.1111/gcb.15958.
39. Virkkala AM, Natali SM, Rogers BM, Watts JD, Savage K, Connon SJ, et al. The ABCflux database: arctic–boreal CO_2 flux observations and ancillary information aggregated to monthly time steps across terrestrial ecosystems. Earth Syst Sci Data. 2022;14(1):179–208. https://doi.org/10.5194/essd-14-179-2022.
40. Dugas WA. Micrometeorological and chamber measurements of CO2 flux from bare soil. Agric For Meteorol. 1993;67(1–2):115–28. https://doi.org/10.1016/0168-1923(93)90053-K.
41. Acosta M, Juszczak R, Chojnicki B, Pavelka M, Havránková K, Lesny J, et al. CO2 fluxes from different vegetation communities on a Peatland ecosystem. Wetlands. 2017;37(3):423–35. https://doi.org/10.1007/s13157-017-0878-4.
42. Goulden ML, Munger JW, Fan SM, Daube BC, Wofsy SC. Measurements of carbon sequestration by long-term eddy covariance: methods and a critical evaluation of accuracy. Glob Change Biol. 1996;2(3):169–82. https://doi.org/10.1111/j.1365-2486.1996.tb00070.x.
43. Baldocchi DD. Assessing the eddy covariance technique for evaluating carbon dioxide exchange rates of ecosystems: past, present and future: carbon balance and Eddy covariance. Glob Change Biol. 2003;9(4):479–92. https://doi.org/10.1046/j.1365-2486.2003.00629.x.
44. Virkkala AM, Virtanen T, Lehtonen A, Rinne J, Luoto M. The current state of CO_2 flux chamber studies in the Arctic tundra: a review. Prog Phys Geogr Earth Environ. 2018;42(2):162–84. https://doi.org/10.1177/0309133317745784.
45. Bjorkman AD, García Criado M, Myers-Smith IH, Ravolainen V, Jónsdóttir IS, Westergaard KB, et al. Status and trends in Arctic vegetation: evidence from experimental warming and long-term

monitoring. Ambio. 2020;49(3):678–92. https://doi.org/10.1007/s13280-019-01161-6.
46. Pallandt MTA, Kumar J, Mauritz M, Schuur EAG, Virkkala AM, Celis G, et al. Representativeness assessment of the pan-Arctic eddy covariance site network and optimized future enhancements. Biogeosciences. 2022;19(3):559–83. https://doi.org/10.5194/bg-19-559-2022.
47. Aubinet M, Grelle A, Ibrom A, Rannik U, Moncrieff J, Foken T, et al. Estimates of the annual net carbon and water exchange of forests: the EUROFLUX methodology. Adv Ecol Res. 1999;30:113–75. https://doi.org/10.1016/S0065-2504(08)60018-5.
48. Valentini R, Matteucci G, Dolman AJ, Schulze ED, Rebmann C, Moors EJ, et al. Respiration as the main determinant of carbon balance in European forests. Nature. 2000;404(6780):861–5. https://doi.org/10.1038/35009084.
49. Yamamoto S, Saigusa N, Gamo M, Fujinuma Y, Inoue G, Hirano T. Findings through the AsiaFlux network and a view toward the future. J Geograph Sci. 2005;15(2):142–8. https://doi.org/10.1007/BF02872679.
50. Dolman AJ, Noilhan J, Durand P, Sarrat C, Brut A, Piguet B, et al. The CarboEurope regional experiment strategy. Bull Am Meterol Soc. 2006;87(10):1367–80. https://doi.org/10.1175/BAMS-87-10-1367.
51. Margolis HA, Flanagan LB, Amiro BD. The Fluxnet-Canada Research network: influence of climate and disturbance on carbon cycling in forests and peatlands. Agric For Meteorol. 2006;140(1–4):1–5. https://doi.org/10.1016/j.agrformet.2006.08.013.
52. Yu G, Wen X, Sun X, Tanner BD, Lee X, Chen J. Overview of ChinaFLUX and evaluation of its eddy covariance measurement. Agric For Meteorol. 2006;137(3–4):125–37. https://doi.org/10.1016/j.agrformet.2006.02.011.
53. Schulze ED, Ciais P, Luyssaert S, Schrumpf M, Janssens IA, Thiruchittampalam B, et al. The European carbon balance. Part 4: integration of carbon and other trace-gas fluxes. Glob Change Biol. 2010;16(5):1451–69. https://doi.org/10.1111/j.1365-2486.2010.02215.x.
54. Restrepo-Coupe N, Da Rocha HR, Hutyra LR, Da Araujo A, Borma LS, Christoffersen B, et al. What drives the seasonality of photosynthesis across the Amazon basin? A cross-site analysis of eddy flux tower measurements from the Brasil flux network. Agric For Meteorol. 2013;182–183:128–44. https://doi.org/10.1016/j.agrformet.2013.04.031.
55. Beringer J, Hutley LB, McHugh I, Arndt SK, Campbell D, Cleugh HA, et al. An introduction to the Australian and New Zealand flux tower network – OzFlux. Biogeosciences. 2016;13(21):5895–916. https://doi.org/10.5194/bg-13-5895-2016.
56. Chu H, Baldocchi DD, John R, Wolf S, Reichstein M. Fluxes all of the time? A primer on the temporal representativeness of FLUXNET: fluxes all of the time? J Geophys Res Biogeosci. 2017;122(2):289–307. https://doi.org/10.1002/2016JG003576.
57. Novick KA, Biederman JA, Desai AR, Litvak ME, Moore DJP, Scott RL, et al. The AmeriFlux network: a coalition of the willing. Agric For Meteorol. 2018;249:444–56. https://doi.org/10.1016/j.agrformet.2017.10.009.
58. Rebmann C, Aubinet M, Schmid H, Arriga N, Aurela M, Burba G, et al. ICOS eddy covariance flux-station site setup: a review. Int Agrophysics. 2018;32(4):471–94. https://doi.org/10.1515/intag-2017-0044.
59. Baldocchi DD. How eddy covariance flux measurements have contributed to our understanding of Global Change Biology. Glob Change Biol. 2020;26(1):242–60. https://doi.org/10.1111/gcb.14807.
60. Stow DA, Hope A, McGuire D, Verbyla D, Gamon J, Huemmrich F, et al. Remote sensing of vegetation and land-cover change in Arctic Tundra Ecosystems. Remote Sens Environ. 2004;89(3):281–308. https://doi.org/10.1016/j.rse.2003.10.018.
61. Sellers PJ, Schimel DS, Moore B, Liu J, Eldering A. Observing carbon cycle–climate feedbacks from space. Proc Natl Acad Sci. 2018;115(31):7860–8. https://doi.org/10.1073/pnas.1716613115.
62. Ryu Y, Berry JA, Baldocchi DD. What is global photosynthesis? History, uncertainties and opportunities. Remote Sens Environ. 2019;223:95–114. https://doi.org/10.1016/j.rse.2019.01.016.
63. Schimel D, Schneider FD, Carbon JPL, Participants E. Flux towers in the sky: global ecology from space. New Phytol. 2019;224(2):570–84. Publisher: Wiley Online Library.
64. Berra EF, Gaulton R. Remote sensing of temperate and boreal forest phenology: a review of progress, challenges and opportunities in the intercomparison of in-situ and satellite phenological metrics. For Ecol Manage. 2021;480:118663. https://doi.org/10.1016/j.foreco.2020.118663.
65. Cheng R, Köehler P, Frankenberg C. Impacts of topography and radiation on temporal upscaling of instantaneous solar-induced chlorophyll fluorescence. Agric For Meteorol. 2022;4:5. https://doi.org/10.1016/j.agrformet.2022.109197.
66. Cheng R, Magney TS, Orcutt EL, Pierrat ZA, Köehler P, Bowling DR, et al. Evaluating photosynthetic activity across Arctic-Boreal land cover types using solar-induced fluorescence. Environ Res Lett. 2022. https://doi.org/10.1088/1748-9326/ac9dae.
67. Demmig-Adams B, Adams WW. The role of xanthophyll cycle carotenoids in the protection of photosynthesis. Trends Plant Sci. 1996;1(1):21–6. https://doi.org/10.1016/S1360-1385(96)80019-7.
68. Tucker CJ. Red and photographic infrared linear combinations for monitoring vegetation. Remote Sens Environ. 1979;8(2):127–50. Publisher: Elsevier.
69. Zeng Y, Hao D, Huete A, Dechant B, Berry J, Chen JM, et al. Optical vegetation indices for monitoring terrestrial ecosystems globally. Nat Rev Earth Environ. 2022;3(7):477–93. https://doi.org/10.1038/s43017-022-00298-5.
70. Huete A, Didan K, Miura T, Rodriguez EP, Gao X, Ferreira LG. Overview of the radiometric and biophysical performance of the MODIS vegetation indices. Remote Sens Environ. 2002;83(1):195–213. https://doi.org/10.1016/S0034-4257(02)00096-2.
71. Gamon J, Huemmrich KF, Wong CYS, Ensminger I, Garrity S, Hollinger DY, et al. A remotely sensed pigment index reveals photosynthetic phenology in evergreen conifers. Proc Natl Acad Sci. 2016;113(46):13087–92. Publisher: National Acad Sciences.
72. Fiore NM, Goulden ML, Czimczik CI, Pedron SA, Tayo MA. Do recent NDVI trends demonstrate boreal forest decline in Alaska? Environ Res Lett. 2020;15(9):095007. https://doi.org/10.1088/1748-9326/ab9c4c.
73. Wang JA, Sulla-Menashe D, Woodcock CE, Sonnentag O, Keeling RF, Friedl MA. Extensive land cover change across Arctic–Boreal Northwestern North America from disturbance and climate forcing. Glob Change Biol. 2020;26(2):807–22. https://doi.org/10.1111/gcb.14804.
74. Sulla-Menashe D, Friedl MA, Krankina ON, Baccini A, Woodcock CE, Sibley A, et al. Hierarchical mapping of Northern Eurasian land cover using MODIS data. Remote Sens Environ. 2011;115(2):392–403. https://doi.org/10.1016/j.rse.2010.09.010.
75. Yang X, Tang J, Mustard JF, Lee JE, Rossini M, Joiner J, et al. Solar-induced chlorophyll fluorescence that correlates with canopy photosynthesis on diurnal and seasonal scales in a temperate deciduous forest: fluorescence and photosynthesis. Geophys Res Lett. 2015;42(8):2977–87. https://doi.org/10.1002/2015GL063201.

76. Gentine P, Alemohammad SH. Reconstructed solar-induced fluorescence: a machine learning vegetation product based on MODIS surface reflectance to reproduce GOME-2 solar-induced fluorescence. Geophys Res Lett. 2018;45(7):3136–46. https://doi.org/10.1002/2017GL076294.
77. Schimel D, Pavlick R, Fisher JB, Asner GP, Saatchi S, Townsend P, et al. Observing terrestrial ecosystems and the carbon cycle from space. Glob Change Biol. 2015;21(5):1762–76. https://doi.org/10.1111/gcb.12822.
78. Porcar-Castell A, Malenovsky Z, Magney T, Van Wittenberghe S, Fernandez-Marin B, Maignan F, et al. Beyond APAR and NPQ: factors coupling and decoupling SIF and GPP across scales. In: 2021 IEEE International Geoscience and Remote Sensing Symposium IGARSS. Brussels, Belgium: IEEE; 2021. pp 1925–1927. Available from: https://ieeexplore.ieee.org/document/9553153/.
79. Guanter L, Frankenberg C, Dudhia A, Lewis PE, Gómez-Dans J, Kuze A, et al. Retrieval and global assessment of terrestrial chlorophyll fluorescence from GOSAT space measurements. Remote Sens Environ. 2012;121:236–51. https://doi.org/10.1016/j.rse.2012.02.006.
80. Zeng Y, Badgley G, Dechant B, Ryu Y, Chen M, Berry JA. A practical approach for estimating the escape ratio of near-infrared solar-induced chlorophyll fluorescence. Remote Sens Environ. 2019;232:111209. https://doi.org/10.1016/j.rse.2019.05.028.
81. Frankenberg C, Fisher JB, Worden J, Badgley G, Saatchi SS, Lee JE, et al. New global observations of the terrestrial carbon cycle from GOSAT: patterns of plant fluorescence with gross primary productivity: Chlorophyll Fluorescence from Space. Geophys Res Lett. 2011;38(17). https://doi.org/10.1029/2011GL048738.
82. Köhler P, Frankenberg C, Magney TS, Guanter L, Joiner J, Landgraf J. Global retrievals of solar-induced chlorophyll fluorescence with TROPOMI: first results and intersensor comparison to OCO-2. Geophys Res Lett. 2018;45(19):10456–63. https://doi.org/10.1029/2018GL079031.
83. Hu J, Liu L, Guo J, Du S, Liu X. Upscaling solar-induced chlorophyll fluorescence from an instantaneous to daily scale gives an improved estimation of the gross primary productivity. Remote Sens. 2018;10(10):1663. https://doi.org/10.3390/rs10101663.
84. Zhang Y, Xiao X, Zhang Y, Wolf S, Zhou S, Joiner J, et al. On the relationship between sub-daily instantaneous and daily total gross primary production: Implications for interpreting satellite-based SIF retrievals. Remote Sens Environ. 2018;205:276–89. https://doi.org/10.1016/j.rse.2017.12.009.
85. Magney TS, Bowling DR, Logan BA, Grossmann K, Stutz J, Blanken PD, et al. Mechanistic evidence for tracking the seasonality of photosynthesis with solar-induced fluorescence. Proc Natl Acad Sci. 2019:201900278. https://doi.org/10.1073/pnas.1900278116.
86. Walther S, Voigt M, Thum T, Gonsamo A, Zhang Y, Köhler P, et al. Satellite chlorophyll fluorescence measurements reveal large-scale decoupling of photosynthesis and greenness dynamics in boreal evergreen forests. Glob Change Biol. 2016;22(9):2979–96. https://doi.org/10.1111/gcb.13200.
87. Zhang Q, Yao T, Huemmrich KF, Middleton E, Lyapustin A, Wang Y. Evaluating impacts of snow, surface water, soil and vegetation on empirical vegetation and snow indices for the Utqiaġvik tundra ecosystem in Alaska with the LVS3 model. Remote Sens Environ. 2020;240:111677. https://doi.org/10.1016/j.rse.2020.111677.
88. Luus KA, Commane R, Parazoo NC, Benmergui J, Euskirchen ES, Frankenberg C, et al. Tundra photosynthesis captured by satellite-observed solar-induced chlorophyll fluorescence. Geophys Res Lett. 2017;44(3):1564–73. Publisher: Wiley Online Library.
89. Jeong S, Schimel D, Frankenberg C, Drewry DT, Fisher JB, Verma M, et al. Application of satellite solar-induced chlorophyll fluorescence to understanding large-scale variations in vegetation phenology and function over northern high latitude forests. Remote Sens Environ. 2017;190:178–87. Publisher: Elsevier.
90. Walther S, Guanter L, Heim B, Jung M, Duveiller G, Wolanin A, et al. Assessing the dynamics of vegetation productivity in circumpolar regions with different satellite indicators of greenness and photosynthesis. Biogeosciences. 2018;15(20):6221–56. https://doi.org/10.5194/bg-15-6221-2018.
91. Maguire AJ, Eitel JUH, Magney TS, Frankenberg C, Köhler P, Orcutt EL, et al. Spatial covariation between solar-induced fluorescence and vegetation indices from Arctic-Boreal landscapes. Environ Res Lett. 2021;16(9):095002. https://doi.org/10.1088/1748-9326/ac188a.
92. Mohammed GH, Colombo R, Middleton EM, Rascher U, van der Tol C, Nedbal L, et al. Remote sensing of solar-induced chlorophyll fluorescence (SIF) in vegetation: 50 years of progress. Remote Sens Environ. 2019;231:111177. https://doi.org/10.1016/j.rse.2019.04.030.
93. Porcar-Castell A, Malenovský Z, Magney T, Van Wittenberghe S, Fernández-Marín B, Maignan F, et al. Chlorophyll a fluorescence illuminates a path connecting plant molecular biology to Earth-system science. Nat Plants. 2021;7(8):998–1009. https://doi.org/10.1038/s41477-021-00980-4.
94. Sun Y, Wen J, Gu L, Joiner J, Chang CY, Van Der Tol C, et al. From remotely-sensed solar-induced chlorophyll fluorescence to ecosystem structure, function, and service: Part II–Harnessing data. Glob Change Biol. 2023;29(11):2893–925. https://doi.org/10.1111/gcb.16646.
95. Tagliabue G, Panigada C, Dechant B, Baret F, Cogliati S, Colombo R, et al. Exploring the spatial relationship between airborne-derived red and far-red sun-induced fluorescence and process-based GPP estimates in a forest ecosystem. Remote Sens Environ. 2019;231:111272. https://doi.org/10.1016/j.rse.2019.111272.
96. Pierrat Z, Nehemy MF, Roy A, Magney T, Parazoo NC, Laroque C, et al. Tower-based remote sensing reveals mechanisms behind a two-phased spring transition in a mixed-species boreal forest. J Geophys Res: Biogeosci. 2021;126(5). https://doi.org/10.1029/2020JG006191.
97. Pierrat ZA, Magney TS, Cheng R, Maguire AJ, Wong CYS, Nehemy MF, et al. The biological basis for using optical signals to track evergreen needleleaf photosynthesis. BioScience. 2024:biad116. https://doi.org/10.1093/biosci/biad116.
98. Parazoo NC, Frankenberg C, Köhler P, Joiner J, Yoshida Y, Magney T, et al. Towards a harmonized long-term spaceborne record of far-red solar-induced fluorescence. J Geophys Res: Biogeosci. 2019;124(8):2518–39. https://doi.org/10.1029/2019JG005289.
99. Joiner J, Guanter L, Lindstrot R, Voigt M, Vasilkov AP, Middleton EM, et al. Global monitoring of terrestrial chlorophyll fluorescence from moderate-spectral-resolution near-infrared satellite measurements: methodology, simulations, and application to GOME-2. Atmos Meas Tech. 2013;6(10):2803–23. https://doi.org/10.5194/amt-6-2803-2013.
100. Joiner J, Yoshida Y, Vasilkov AP, Middleton EM, et al. First observations of global and seasonal terrestrial chlorophyll fluorescence from space. Biogeosciences. 2011;8(3):637. Publisher: Copernicus GmbH.
101. Köhler P, Guanter L, Joiner J. A linear method for the retrieval of sun-induced chlorophyll fluorescence from GOME-2 and SCIAMACHY data. Atmos Meas Tech. 2015;8(6):2589–608. https://doi.org/10.5194/amt-8-2589-2015.
102. Sun Y, Frankenberg C, Wood JD, Schimel DS, Jung M, Guanter L, et al. OCO-2 advances photosynthesis observation from space via solar-induced chlorophyll fluorescence. Science. 2017;358(6360). Publisher: American Association for the Advancement of Science. https://doi.org/10.1126/science.aam5747.

103. Du S, Liu L, Liu X, Zhang X, Zhang X, Bi Y, et al. Retrieval of global terrestrial solar-induced chlorophyll fluorescence from TanSat satellite. Sci Bull. 2018;63(22):1502–12. https://doi.org/10.1016/j.scib.2018.10.003.
104. Wang JA, Sulla-Menashe D, Woodcock CE, Sonnentag O, Keeling RF, Friedl MA. ABoVE: Landsat-derived Annual Dominant Land Cover Across ABoVE Core Domain, 1984–2014. ORNL DAAC; 2019. https://doi.org/10.3334/ORNLDAAC/1691.
105. Muster S, Langer M, Heim B, Westermann S, Boike J. Subpixel heterogeneity of ice-wedge polygonal tundra: a multi-scale analysis of land cover and evapotranspiration in the Lena River Delta, Siberia. Tellus B: Chem Phys Meteorol. 2012;64(1):17301. https://doi.org/10.3402/tellusb.v64i0.17301.
106. Treat CC, Marushchak ME, Voigt C, Zhang Y, Tan Z, Zhuang Q, et al. Tundra landscape heterogeneity, not interannual variability, controls the decadal regional carbon balance in the Western Russian Arctic. Glob Change Biol. 2018;24(11):5188–204. https://doi.org/10.1111/gcb.14421.
107. Siewert MB, Olofsson J. Scale-dependency of Arctic ecosystem properties revealed by UAV. Environ Res Lett. 2020;15(9):094030. https://doi.org/10.1088/1748-9326/aba20b.
108. Juutinen S, Aurela M, Tuovinen JP, Ivakhov V, Linkosalmi M, Räsänen A, et al. Variation in CO_2 and CH_4 fluxes among land cover types in heterogeneous Arctic tundra in northeastern Siberia. Biogeosciences. 2022;19(13):3151–67. https://doi.org/10.5194/bg-19-3151-2022.
109. Joiner J, Vasilkov AP, Middleton EM, Campbell PKE, Yoshida Y, Yoshida Y, et al. Filling-in of near-infrared solar lines by terrestrial fluorescence and other geophysical effects: simulations and space-based observations from SCIAMACHY and GOSAT. Atmos Meas Tech. 2012;5(4):809–29. https://doi.org/10.5194/amt-5-809-2012.
110. Coppo P, Taiti A, Pettinato L, Francois M, Taccola M, Drusch M. Fluorescence Imaging Spectrometer (FLORIS) for ESA FLEX Mission. Remote Sens. 2017;9(7):649. https://doi.org/10.3390/rs9070649.
111. Kraft S, Del Bello U, Bouvet M, Drusch M, Moreno J. FLEX: ESA's Earth Explorer 8 candidate mission. In: EEE International Geoscience and Remote Sensing Symposium. Munich, Germany: IEEE; 2012. pp. 7125–7128. ISSN: 2153-7003. Available from: https://ieeexplore.ieee.org/document/6352020.
112. Duveiller G, Cescatti A. Spatially downscaling sun-induced chlorophyll fluorescence leads to an improved temporal correlation with gross primary productivity. Remote Sens Environ. 2016;182:72–89. https://doi.org/10.1016/j.rse.2016.04.027.
113. Zhang Y, Joiner J, Alemohammad SH, Zhou S, Gentine P. A global spatially contiguous solar-induced fluorescence (CSIF) dataset using neural networks. Biogeosciences. 2018;15(19):5779–800. https://doi.org/10.5194/bg-15-5779-2018.
114. Li X, Xiao J. A Global, 0.05-Degree Product of Solar-Induced Chlorophyll Fluorescence Derived from OCO-2, MODIS, and Reanalysis Data. Remote Sens. 2019;11(5):517. https://doi.org/10.3390/rs11050517.
115. Duveiller G, Filipponi F, Walther S, Köhler P, Frankenberg C, Guanter L, et al. A spatially downscaled sun-induced fluorescence global product for enhanced monitoring of vegetation productivity. Earth Syst Sci Data. 2020;12(2):1101–16. https://doi.org/10.5194/essd-12-1101-2020.
116. Turner AJ, Köhler P, Magney TS, Frankenberg C, Fung I, Cohen RC. A double peak in the seasonality of California's photosynthesis as observed from space. Biogeosciences. 2020;17(2):405–22. https://doi.org/10.5194/bg-17-405-2020.
117. Gensheimer J, Turner AJ, Köhler P, Frankenberg C, Chen J. A convolutional neural network for spatial downscaling of satellite-based solar-induced chlorophyll fluorescence (SIFnet). Biogeosciences. 2022;19(6):1777–93. https://doi.org/10.5194/bg-19-1777-2022.
118. Madani N, Parazoo NC, Miller CE. Climate change is enforcing physiological changes in Arctic Ecosystems. Environ Res Lett. 2023;18(7):074027. https://doi.org/10.1088/1748-9326/acde92.
119. Wen J, Köhler P, Duveiller G, Parazoo NC, Magney TS, Hooker G, et al. A framework for harmonizing multiple satellite instruments to generate a long-term global high spatial-resolution solar-induced chlorophyll fluorescence (SIF). Remote Sens Environ. 2020;239:111644. https://doi.org/10.1016/j.rse.2020.111644.
120. Randerson JT, Thompson MV, Conway TJ, Fung IY, Field CB. The contribution of terrestrial sources and sinks to trends in the seasonal cycle of atmospheric carbon dioxide. Glob Biogeochem Cycles. 1997;11(4):535–60. https://doi.org/10.1029/97GB02268.
121. Birch L, Schwalm CR, Natali S, Lombardozzi D, Keppel-Aleks G, Watts J, et al. Addressing biases in Arctic–boreal carbon cycling in the Community Land Model Version 5. Geosci Model Dev. 2021;14(6):3361–82. https://doi.org/10.5194/gmd-14-3361-2021.
122. Arndt KA, Hashemi J, Natali SM, Schiferl LD, Virkkala AM. Recent advances and challenges in monitoring and modeling non-growing season carbon dioxide fluxes from the arctic boreal zone. Curr Clim Change Rep. 2023;9(2):27–40. https://doi.org/10.1007/s40641-023-00190-4.
123. Parazoo NC, Bowman K, Fisher JB, Frankenberg C, Jones DBA, Cescatti A, et al. Terrestrial gross primary production inferred from satellite fluorescence and vegetation models. Glob Change Biol. 2014;20(10):3103–21. https://doi.org/10.1111/gcb.12652.
124. Byrne B, Liu J, Yi Y, Chatterjee A, Basu S, Cheng R, et al. Multiyear observations reveal a larger than expected autumn respiration signal across northeast Eurasia. Biogeosci Discuss. 2022; 1–28. Publisher: Copernicus GmbH. https://doi.org/10.5194/bg-2022-40.
125. Zhang Z, Guanter L, Porcar-Castell A, Rossini M, Pacheco-Labrador J, Zhang Y. Global modeling diurnal gross primary production from OCO-3 solar-induced chlorophyll fluorescence. Remote Sens Environ. 2023;285:113383. https://doi.org/10.1016/j.rse.2022.113383.
126. Zhang Z, Zhang Y. Solar angle matters: diurnal pattern of solar-induced chlorophyll fluorescence from OCO-3 and TROPOMI. Remote Sens Environ. 2023;285:113380. https://doi.org/10.1016/j.rse.2022.113380.
127. Somkuti P, O'Dell CW, Crowell S, Köhler P, McGarragh GR, Cronk HQ, et al. Solar-induced chlorophyll fluorescence from the Geostationary Carbon Cycle Observatory (GeoCarb): an extensive simulation study. Remote Sens Environ. 2021;263:112565. https://doi.org/10.1016/j.rse.2021.112565.
128. Joiner J, Yoshida Y, Koehler P, Frankenberg C, Parazoo NC. SIF-ESDRL2 Solar-Induced Fluorescence (SIF) from SCIAMACHY, 2003-2012. Available from: https://daac.ornl.gov/cgi-bin/dsviewer.pl?ds_id=1871.
129. Doughty R, Kurosu T, Parazoo N, Köhler P, Wang Y, Sun Y, et al. Global GOSAT, OCO-2 and OCO-3 Solar Induced Chlorophyll Fluorescence Datasets. Biosphere – Biogeosciences; 2021. Available from: https://essd.copernicus.org/preprints/essd-2021-237/essd-2021-237.pdf.
130. Suto H, Kataoka F, Kikuchi N, Knuteson RO, Butz A, Haun M, et al. Thermal and near-infrared sensor for carbon observation Fourier transform spectrometer-2 (TANSO-FTS-2) on the Greenhouse gases Observing SATellite-2 (GOSAT-2) during its first year in orbit. Atmos Meas Tech. 2021;14(3):2013–39. https://doi.org/10.5194/amt-14-2013-2021.
131. Frankenberg C, O'Dell C, Berry J, Guanter L, Joiner J, Köhler P, et al. Prospects for chlorophyll fluorescence remote sensing

from the Orbiting Carbon Observatory-2. Remote Sens Environ. 2014;147:1–12. Publisher: Elsevier.
132. Guanter L, Bacour C, Schneider A, Aben I, Van Kempen TA, Maignan F, et al. The TROPOSIF global sun-induced fluorescence dataset from the Sentinel-5P TROPOMI mission. Earth Syst Sci Data. 2021;13(11):5423–40. https://doi.org/10.5194/essd-13-5423-2021.
133. Zoogman P, Liu X, Suleiman RM, Pennington WF, Flittner DE, Al-Saadi JA, et al. Tropospheric emissions: monitoring of pollution (TEMPO). J Quant Spectrosc Radiat Transfer. 2017;186:17–39. https://doi.org/10.1016/j.jqsrt.2016.05.008.
134. Kolm MG, Maurer R, Sallusti M, Bagnasco G, Gulde ST, Smith DJ, et al. Sentinel 4: a geostationary imaging UVN spectrometer for air quality monitoring: status of design, performance and development. In: Cugny B, Sodnik Z, Karafolas N, editors. International Conference on Space Optics – ICSO 2014. Tenerife, Canary Islands, Spain: SPIE; 2017. pp 39. Available from: https://www.spiedigitallibrary.org/conference-proceedings-of-spie/10563/2304099/Sentinel-4--a-geostationary-imaging-UVN-spectrometer-for-air/10.1117/12.2304099.full.
135. Bazalgette Courrèges-Lacoste G, Bagnasco G, Bulsa G, Riedl S, Smith D, Maurer R, et al. The Copernicus Sentinel 4 mission: a geostationary imaging UVN spectrometer for air quality monitoring. In: Meynart R, Neeck SP, Shimoda H, Kimura T, Bézy JL, editors. Sensors, Systems, and Next-Generation Satellites XXI. Warsaw, Poland: SPIE; 2017. pp 6. Available from: https://www.spiedigitallibrary.org/conference-proceedings-of-spie/10423/2282158/The-Copernicus-Sentinel-4-mission--a-geostationary-imaging-UVN/10.1117/12.2282158.full.
136. Sierk B, Fernandez V, Bézy JL, Meijer Y, Durand Y, Bazalgette Courrèges-Lacoste G, et al. The Copernicus CO2M mission for monitoring anthropogenic carbon dioxide emissions from space. In: Sodnik Z, Cugny B, Karafolas N, editors. International Conference on Space Optics – ICSO 2020. Online Only, France: SPIE; 2021. p 128. Available from: https://www.spiedigitallibrary.org/conference-proceedings-of-spie/11852/2599613/The-Copernicus-CO2M-mission-for-monitoring-anthropogenic-carbon-dioxide-emissions/10.1117/12.2599613.full.
137. Wang R, Gamon JA, Hmimina G, Cogliati S, Zygielbaum AI, Arkebauer TJ, et al. Harmonizing solar induced fluorescence across spatial scales, instruments, and extraction methods using proximal and airborne remote sensing: a multi-scale study in a soybean field. Remote Sens Environ. 2022;281:113268. https://doi.org/10.1016/j.rse.2022.113268.
138. Frankenberg C, Köhler P, Magney TS, Geier S, Lawson P, Schwochert M, et al. The Chlorophyll Fluorescence Imaging Spectrometer (CFIS), mapping far red fluorescence from aircraft. Remote Sens Environ. 2018;217:523–36. https://doi.org/10.1016/j.rse.2018.08.032.
139. Miller CE, Griffith PC, Goetz SJ, Hoy EE, Pinto N, McCubbin IB, et al. An overview of ABoVE airborne campaign data acquisitions and science opportunities. Environ Res Lett. 2019;14(8):080201. https://doi.org/10.1088/1748-9326/ab0d44.
140. Drewry D, Miller CE, Frankenberg C, Euskirchen ES, Rocha AV, Bret-Harte MS, et al. Airborne Solar-Induced Chlorophyll Fluorescence to Characterize Arctic Boreal Zone Productivity. Washington D.C.; 2019. Available from: https://ui.adsabs.harvard.edu/abs/2019AGUFM.B14D..03D/abstract.
141. Orcutt E, Frankenberg C, Housen C, Arndt K, Euskirchen E, Hould Gosselin G, et al. Footprints in the tundra: Considerations for linking remote sensing observations with flux tower data in the Arctic-Boreal Zone. New Orleans, LA; 2021. Available from: https://ui.adsabs.harvard.edu/abs/2021AGUFM.B13D..05O/abstract.
142. Gamon JA. Reviews and Syntheses: optical sampling of the flux tower footprint. Biogeosciences. 2015;12(14):4509–23. https://doi.org/10.5194/bg-12-4509-2015.
143. Chu H, Luo X, Ouyang Z, Chan WS, Dengel S, Biraud SC, et al. Representativeness of Eddy-Covariance flux footprints for areas surrounding AmeriFlux sites. Agric For Meteorol. 2021;301–302:108350. https://doi.org/10.1016/j.agrformet.2021.108350.
144. Pierrat Z, Magney T, Parazoo NC, Grossmann K, Bowling DR, Seibt U, et al. Diurnal and Seasonal Dynamics of Solar-Induced Chlorophyll Fluorescence, Vegetation Indices, and Gross Primary Productivity in the Boreal Forest. J Geophys Res: Biogeosci. 2022;127(2):3. https://doi.org/10.1029/2021JG006588.
145. Yang X, Shi H, Stovall A, Guan K, Miao G, Zhang Y, et al. FluoSpec 2–An Automated Field Spectroscopy System to Monitor Canopy Solar-Induced Fluorescence. Sensors. 2018;18(7):2063. https://doi.org/10.3390/s18072063.
146. Wong CYS, Jones T, McHugh DP, Gilbert ME, Gepts P, Palkovic A, et al. TSWIFT: Tower Spectrometer on Wheels for Investigating Frequent Timeseries for high-throughput phenotyping of vegetation physiology. Plant Methods. 2023;19(1):29. https://doi.org/10.1186/s13007-023-01001-5.
147. Gu L, Wood JD, Chang CYY, Sun Y, Riggs JS. Advancing terrestrial ecosystem science with a novel automated measurement system for sun-induced chlorophyll fluorescence for integration with Eddy covariance flux networks. J Geophys Res: Biogeosci. 2019;124(1):127–46. https://doi.org/10.1029/2018JG004742.
148. Guanter L, Rossini M, Colombo R, Meroni M, Frankenberg C, Lee JE, et al. Using field spectroscopy to assess the potential of statistical approaches for the retrieval of sun-induced chlorophyll fluorescence from ground and space. Remote Sens Environ. 2013;133:52–61. https://doi.org/10.1016/j.rse.2013.01.017.
149. Grossmann K, Frankenberg C, Magney TS, Hurlock SC, Seibt U, Stutz J. PhotoSpec: a new instrument to measure spatially distributed red and far-red Solar-Induced Chlorophyll Fluorescence. Remote Sens Environ. 2018;216:311–27. https://doi.org/10.1016/j.rse.2018.07.002.
150. Shuai Y, Schaaf CB, Strahler AH, Liu J, Jiao Z. Quality assessment of BRDF/albedo retrievals in MODIS operational system. Geophys Res Lett. 2008;35(5):L05407. https://doi.org/10.1029/2007GL032568.
151. Hao D, Zeng Y, Qiu H, Biriukova K, Celesti M, Migliavacca M, et al. Practical approaches for normalizing directional solar-induced fluorescence to a standard viewing geometry. Remote Sens Environ. 2021;255:112171. https://doi.org/10.1016/j.rse.2020.112171.
152. Atherton J, MacArthur A, Hakala T, Maseyk K, Robinson I, Liu W, et al. Drone measurements of solar-induced chlorophyll fluorescence acquired with a low-weight DFOV spectrometer system. In: IGARSS 2018 - 2018 IEEE International Geoscience and Remote Sensing Symposium. Valencia: IEEE; 2018. pp 8834–8836. Available from: https://ieeexplore.ieee.org/document/8517474/.
153. Wang N, Clevers JGPW, Wieneke S, Bartholomeus H, Kooistra L. Potential of UAV-based sun-induced chlorophyll fluorescence to detect water stress in sugar beet. Agric For Meteorol. 2022;323:109033. https://doi.org/10.1016/j.agrformet.2022.109033.
154. Gamon J, Rahman A, Dungan J, Schildhauer M, Huemmrich K. Spectral Network (SpecNet)-What is it and why do we need it? Remote Sens Environ. 2006;103(3):227–35. https://doi.org/10.1016/j.rse.2006.04.003.
155. Gamon JA, Coburn C, Flanagan LB, Huemmrich KF, Kiddle C, Sanchez-Azofeifa GA, et al. SpecNet revisited: bridging flux and remote sensing communities. Can J Remote Sens. 2010;36(sup2):S376–90. https://doi.org/10.5589/m10-067.
156. Julitta T, Corp L, Rossini M, Burkart A, Cogliati S, Davies N, et al. Comparison of sun-induced chlorophyll fluorescence estimates

obtained from four portable field spectroradiometers. Remote Sens. 2016;8(2):122. https://doi.org/10.3390/rs8020122.
157. Kim J, Ryu Y, Dechant B. Development of a filter-based near-surface remote sensing system to retrieve far-red sun-induced chlorophyll fluorescence. Remote Sens Environ. 2022;283:113311. https://doi.org/10.1016/j.rse.2022.113311.
158. Turner AJ, Köhler P, Magney TS, Frankenberg C, Fung I, Cohen RC. Extreme events driving year-to-year differences in gross primary productivity across the US. Biogeosciences. 2021;18(24):6579–88. https://doi.org/10.5194/bg-18-6579-2021.
159. Damm A, Guanter L, Paul-Limoges E, Van Der Tol C, Hueni A, Buchmann N, et al. Far-red sun-induced chlorophyll fluorescence shows ecosystem-specific relationships to gross primary production: an assessment based on observational and modeling approaches. Remote Sens Environ. 2015;166:91–105. https://doi.org/10.1016/j.rse.2015.06.004.
160. Magney TS, Barnes ML, Yang X. On the Covariation of Chlorophyll Fluorescence and Photosynthesis Across Scales. Geophys Res Lett. 2020;47(23). https://doi.org/10.1029/2020GL091098.
161. Sun Y, Frankenberg C, Jung M, Joiner J, Guanter L, Köhler P, et al. Overview of Solar-Induced chlorophyll Fluorescence (SIF) from the Orbiting Carbon Observatory-2: Retrieval, cross-mission comparison, and global monitoring for GPP. Remote Sens Environ. 2018;209:808–23. https://doi.org/10.1016/j.rse.2018.02.016.
162. Liu Y, Chen JM, He L, Zhang Z, Wang R, Rogers C, et al. Non-linearity between gross primary productivity and far-red solar-induced chlorophyll fluorescence emitted from canopies of major biomes. Remote Sens Environ. 2022;271:112896. https://doi.org/10.1016/j.rse.2022.112896.
163. Li X, Xiao J. TROPOMI observations allow for robust exploration of the relationship between solar-induced chlorophyll fluorescence and terrestrial gross primary production. Remote Sens Environ. 2022;268:112748. https://doi.org/10.1016/j.rse.2021.112748.
164. Hiyama T, Ueyama M, Kotani A, Iwata H, Nakai T, Okamura M, et al. Lessons learned from more than a decade of greenhouse gas flux measurements at boreal forests in eastern Siberia and interior Alaska. Polar Sci. 2021;27:100607. https://doi.org/10.1016/j.polar.2020.100607.
165. Jung M, Schwalm C, Migliavacca M, Walther S, Camps-Valls G, Koirala S, et al. Scaling carbon fluxes from eddy covariance sites to globe: synthesis and evaluation of the FLUXCOM approach. Biogeosciences. 2020;17(5):1343–65. Publisher: Copernicus GmbH on behalf of the European Geosciences Union.
166. Chen A, Mao J, Ricciuto D, Xiao J, Frankenberg C, Li X, et al. Moisture availability mediates the relationship between terrestrial gross primary production and solar-induced chlorophyll fluorescence: Insights from global-scale variations. Glob Change Biol. 2021;27(6):1144–56. https://doi.org/10.1111/gcb.15373.
167. Chen A, Mao J, Ricciuto D, Lu D, Xiao J, Li X, et al. Seasonal changes in GPP/SIF ratios and their climatic determinants across the Northern Hemisphere. Glob Change Biol. 2021;27(20):5186–97. https://doi.org/10.1111/gcb.15775.
168. Yang D, Morrison BD, Hantson W, Breen AL, McMahon A, Li Q, et al. Landscape-scale characterization of Arctic tundra vegetation composition, structure, and function with a multi-sensor unoccupied aerial system. Environ Res Lett. 2021;16(8):085005. https://doi.org/10.1088/1748-9326/ac1291.
169. Paul-Limoges E, Damm A, Hueni A, Liebisch F, Eugster W, Schaepman M, et al. Effect of environmental conditions on sun-induced fluorescence in a mixed forest and a cropland. Remote Sens Environ. 2018;219:310–23. https://doi.org/10.1016/j.rse.2018.10.018.
170. Chen R, Liu L, Liu X. Leaf chlorophyll contents dominates the seasonal dynamics of SIF/GPP ratio: evidence from continuous measurements in a maize field. Agric For Meteorol. 2022;323:109070. https://doi.org/10.1016/j.agrformet.2022.109070.
171. Zhang Z, Zhang Y, Porcar-Castell A, Joiner J, Guanter L, Yang X, et al. Reduction of structural impacts and distinction of photosynthetic pathways in a global estimation of GPP from space-borne solar-induced chlorophyll fluorescence. Remote Sens Environ. 2020;240:111722. https://doi.org/10.1016/j.rse.2020.111722.
172. Joiner J, Yoshida Y. Satellite-based reflectances capture large fraction of variability in global gross primary production (GPP) at weekly time scales. Agric For Meteorol. 2020;291:108092. Publisher: Elsevier.
173. He W, Ju W, Jiang F, Parazoo N, Gentine P, Wu X, et al. Peak growing season patterns and climate extremes-driven responses of gross primary production estimated by satellite and process based models over North America. Agric For Meteorol. 2021;298–299:108292. https://doi.org/10.1016/j.agrformet.2020.108292.
174. Joiner J, Yoshida Y, Zhang Y, Duveiller G, Jung M, Lyapustin A, et al. Estimation of terrestrial global gross primary production (GPP) with satellite data-driven models and Eddy covariance flux data. Remote Sens. 2018;10(9):1346. https://doi.org/10.3390/rs10091346.
175. Joiner, J , Yoshida, Y .: Vegetation CollectionGlobal MODIS and FLUXNET-derived Daily Gross Primary Production, V2. Available from: https://daac.ornl.gov/cgi-bin/dsviewer.pl?ds_id=1835.
176. Pitman AJ. The evolution of, and revolution in, land surface schemes designed for climate models. Int J Climatol. 2003;23(5):479–510. https://doi.org/10.1002/joc.893.
177. Williams M, Richardson AD, Reichstein M, Stoy PC, Peylin P, Verbeeck H, et al. Improving land surface models with FLUXNET data. Biogeosciences. 2009;6(7):1341–59. https://doi.org/10.5194/bg-6-1341-2009.
178. MacBean N, Maignan F, Bacour C, Lewis P, Peylin P, Guanter L, et al. Strong constraint on modelled global carbon uptake using solar-induced chlorophyll fluorescence data. Sci Rep. 2018;8(1):1973. https://doi.org/10.1038/s41598-018-20024-w.
179. Forkel M, Drüke M, Thurner M, Dorigo W, Schaphoff S, Thonicke K, et al. Constraining modelled global vegetation dynamics and carbon turnover using multiple satellite observations. Sci Rep. 2019;9(1):18757. https://doi.org/10.1038/s41598-019-55187-7.
180. Wang J, Jiang F, Wang H, Qiu B, Wu M, He W, et al. Constraining global terrestrial gross primary productivity in a global carbon assimilation system with OCO-2 chlorophyll fluorescence data. Agric For Meteorol. 2021;304–305:108424. https://doi.org/10.1016/j.agrformet.2021.108424.
181. Norton AJ, Rayner PJ, Koffi EN, Scholze M, Silver DD, Wang YP. Estimating global gross primary productivity using chlorophyll fluorescence and a data assimilation system with the BETHY-SCOPE model. Biogeosciences. 2019;16(15):3069–93. https://doi.org/10.5194/bg-16-3069-2019.
182. Han J, Chang CYY, Gu L, Zhang Y, Meeker EW, Magney TS, et al. The physiological basis for estimating photosynthesis from Chl a fluorescence. New Phytol. 2022;234(4):1206–19. https://doi.org/10.1111/nph.18045.
183. Chen A, Ricciuto D, Mao J, Wang J, Lu D, Meng F. Improving E3SM land model photosynthesis parameterization via satellite SIF, machine learning, and surrogate modeling. J Adv Model Earth Syst. 2023;15(4):e2022MS003135. https://doi.org/10.1029/2022MS003135.
184. Raczka B, Porcar-Castell A, Magney T, Lee JE, Köhler P, Frankenberg C, et al. Sustained nonphotochemical quenching shapes the seasonal pattern of solar-induced fluorescence at a

high-elevation evergreen forest. J Geophys Res: Biogeosciences. 2019;124(7):2005–20. https://doi.org/10.1029/2018JG004883.

185. Li R, Lombardozzi D, Shi M, Frankenberg C, Parazoo NC, Köhler P, et al. Representation of leaf-to-canopy radiative transfer processes improves simulation of far-red solar-induced chlorophyll fluorescence in the community land model version 5. J Adv Model Earth Syst. 2022;14(3):e2021MS002747. https://doi.org/10.1029/2021MS002747.
186. Thum T, Zaehle S, Köhler P, Aalto T, Aurela M, Guanter L, et al. Modelling sun-induced fluorescence and photosynthesis with a land surface model at local and regional scales in Northern Europe. Biogeosciences. 2017;14(7):1969–87. Publisher: Copernicus GmbH on behalf of the European Geosciences Union.
187. Shiga YP, Tadić JM, Qiu X, Yadav V, Andrews AE, Berry JA, et al. Atmospheric CO_2 observations reveal strong correlation between regional net biospheric carbon uptake and solar-induced chlorophyll fluorescence. Geophys Res Lett. 2018;45(2):1122–32. https://doi.org/10.1002/2017GL076630.
188. Wang Y, Braghiere RK, Longo M, Norton AJ, Köhler P, Doughty R, et al. Modeling global vegetation gross primary productivity, transpiration and hyperspectral canopy radiative transfer simultaneously using a next generation land surface model-CliMA land. J Adv Model Earth Syst. 2023;15(3):e2021MS002964. https://doi.org/10.1029/2021MS002964.
189. Beamish A, Raynolds MK, Epstein H, Frost GV, Macander MJ, Bergstedt H, et al. Recent trends and remaining challenges for optical remote sensing of Arctic tundra vegetation: a review and outlook. Remote Sens Environ. 2020;246:111872. https://doi.org/10.1016/j.rse.2020.111872.
190. Jia GJ, Epstein HE, Walker DA. Greening of arctic Alaska, 1981–2001. Geophysical Research Letters. 2003;30(20):2003GL018268. https://doi.org/10.1029/2003GL018268.
191. Park T, Ganguly S, Tømmervik H, Euskirchen ES, Høgda KA, Karlsen SR, et al. Changes in growing season duration and productivity of northern vegetation inferred from long-term remote sensing data. Environ Res Lett. 2016;11(8):084001. Publisher: IOP Publishing.
192. Arndt KA, Santos MJ, Ustin S, Davidson SJ, Stow D, Oechel WC, et al. Arctic greening associated with lengthening growing seasons in Northern Alaska. Environ Res Lett. 2019;14(12):125018. https://doi.org/10.1088/1748-9326/ab5e26.
193. Li X, Xiao J. Global climatic controls on interannual variability of ecosystem productivity: similarities and differences inferred from solar-induced chlorophyll fluorescence and enhanced vegetation index. Agric For Meteorol. 2020;288–289:108018. https://doi.org/10.1016/j.agrformet.2020.108018.
194. Liu Z, Kimball JS, Parazoo NC, Ballantyne AP, Wang WJ, Madani N, et al. Increased high-latitude photosynthetic carbon gain offset by respiration carbon loss during an anomalous warm winter to spring transition. Glob Change Biol. 2020;26(2):682–96. https://doi.org/10.1111/gcb.14863.
195. Zhang W, Jin H, Jamali S, Duan Z, Wu M, Ran Y, et al. Convergence and divergence emerging in climatic controls of polynomial trends for northern ecosystem productivity over 2000–2018. Sci Total Environ. 2023;874:162425. https://doi.org/10.1016/j.scitotenv.2023.162425.
196. Walther S, Duveiller G, Jung M, Guanter L, Cescatti A, Camps-Valls G. Satellite Observations of the Contrasting Response of Trees and Grasses to Variations in Water Availability. Geophys Res Lett. 2019;46(3):1429–40. https://doi.org/10.1029/2018GL080535.
197. Lu X, Cheng X, Li X, Chen J, Sun M, Ji M, et al. Seasonal patterns of canopy photosynthesis captured by remotely sensed sun-induced fluorescence and vegetation indexes in mid-to-high latitude forests: a cross-platform comparison. Sci Total Environ. 2018;644:439–51. https://doi.org/10.1016/j.scitotenv.2018.06.269.
198. Parazoo NC, Arneth A, Pugh TAM, Smith B, Steiner N, Luus K, et al. Spring photosynthetic onset and net CO$_2$ uptake in Alaska triggered by landscape thawing. Glob Change Biol. 2018;24(8):3416–35. https://doi.org/10.1111/gcb.14283.
199. Kim Y, Kimbal JS, Parazoo N, Xu X, Dunbar RS, Colliander A, et al. Monitoring ECO-Hydrological Spring Onset Over Alaska and Northern Canada with Complementary Satellite Remote Sensing Data. In: 2021 IEEE International Geoscience and Remote Sensing Symposium IGARSS. Brussels, Belgium: IEEE; 2021. pp. 6363–6366. Available from: https://ieeexplore.ieee.org/document/9553220/.
200. Bowling DR, Logan BA, Hufkens K, Aubrecht DM, Richardson AD, Burns SP, et al. Limitations to winter and spring photosynthesis of a Rocky Mountain subalpine forest. Agric For Meteorol. 2018;252:241–55. https://doi.org/10.1016/j.agrformet.2018.01.025.
201. Zhou S, Zhang Y, Ciais P, Xiao X, Luo Y, Caylor KK, et al. Dominant role of plant physiology in trend and variability of gross primary productivity in North America. Sci Rep. 2017;7(1):41366. https://doi.org/10.1038/srep41366.
202. Butterfield Z, Buermann W, Keppel-Aleks G. Satellite observations reveal seasonal redistribution of Northern ecosystem productivity in response to interannual climate variability. Remote Sens Environ. 2020;242:111755. https://doi.org/10.1016/j.rse.2020.111755.
203. Shi M, Parazoo NC, Jeong SJ, Birch L, Lawrence P, Euskirchen ES, et al. Exposure to cold temperature affects the spring phenology of Alaskan deciduous vegetation types. Environ Res Lett. 2020;15(2):025006. https://doi.org/10.1088/1748-9326/ab6502.
204. Yang JC, Magney TS, Albert LP, Richardson AD, Frankenberg C, Stutz J, et al. Gross Primary Production (GPP) and red solar induced fluorescence (SIF) respond differently to light and seasonal environmental conditions in a subalpine conifer forest. Agric For Meteorol. 2022;317:108904. https://doi.org/10.1016/j.agrformet.2022.108904.
205. Zhang Y, Parazoo NC, Williams AP, Zhou S, Gentine P. Large and projected strengthening moisture limitation on end-of-season photosynthesis. Proc Natl Acad Sci. 2020;117(17):9216–22. https://doi.org/10.1073/pnas.1914436117.
206. Nehemy MF, Pierrat Z, Maillet J, Richardson AD, Stutz J, Johnson B, et al. Phenological assessment of transpiration: the stem-temp approach for determining start and end of season. Agric For Meteorol. 2023;331:109319. https://doi.org/10.1016/j.agrformet.2023.109319.
207. Jonard F, Feldman AF, Short Gianotti DJ, Entekhabi D. Observed water and light limitation across global ecosystems. Biogeosciences. 2022;19(23):5575–90. https://doi.org/10.5194/bg-19-5575-2022.
208. Descals A, Verger A, Yin G, Filella I, Fu YH, Piao S, et al. Radiation-constrained boundaries cause nonuniform responses of the carbon uptake phenology to climatic warming in the Northern Hemisphere. Glob Change Biol. 2023;29(3):719–30. https://doi.org/10.1111/gcb.16502.
209. Zhang Y, Commane R, Zhou S, Williams AP, Gentine P. Light limitation regulates the response of autumn terrestrial carbon uptake to warming. Nat Clim Change. 2020;10(8):739–43. https://doi.org/10.1038/s41558-020-0806-0.
210. Wulder MA, Roy DP, Radeloff VC, Loveland TR, Anderson MC, Johnson DM, et al. Fifty years of Landsat science and impacts. Remote Sens Environ. 2022;280:113195. https://doi.org/10.1016/j.rse.2022.113195.
211. Park T, Chen C, Macias-Fauria M, Tømmervik H, Choi S, Winkler A, et al. Changes in timing of seasonal peak photo-

synthetic activity in northern ecosystems. Glob Change Biol. 2019;25(7):2382–95. https://doi.org/10.1111/gcb.14638.
212. Liu J, Wennberg PO, Parazoo NC, Yin Y, Frankenberg C. Observational constraints on the response of high-latitude Northern forests to warming. AGU Adv. 2020;1(4). https://doi.org/10.1029/2020AV000228.
213. Madani N, Parazoo NC, Kimball JS, Reichle RH, Chatterjee A, Watts JD, et al. The impacts of climate and wildfire on ecosystem gross primary productivity in Alaska. J Geophys Res: Biogeosciences. 2021;126(6). https://doi.org/10.1029/2020JG006078.
214. Wang T, Liu D, Piao S, Wang Y, Wang X, Guo H, et al. Emerging negative impact of warming on summer carbon uptake in northern ecosystems. Nat Commun. 2018;9(1):5391. https://doi.org/10.1038/s41467-018-07813-7.
215. Yin G, Verger A, Descals A, Filella I, Peñuelas J. Nonlinear Thermal responses outweigh water limitation in the attenuated effect of climatic warming on photosynthesis in Northern ecosystems. Geophys Res Lett. 2022;49(16). https://doi.org/10.1029/2022GL100096.
216. Zhao Q, Zhu Z, Zeng H, Myneni RB, Zhang Y, Peñuelas J, et al. Seasonal peak photosynthesis is hindered by late canopy development in northern ecosystems. Nat Plants. 2022;8(12):1484–92. https://doi.org/10.1038/s41477-022-01278-9.
217. Magney TS, Frankenberg C, Köhler P, North G, Davis TS, Dold C, et al. Disentangling changes in the spectral shape of chlorophyll fluorescence: implications for remote sensing of photosynthesis. J Geophys Res: Biogeosciences. 2019;124(6):1491–507. https://doi.org/10.1029/2019JG005029.
218. Serbin SP, Singh A, McNeil BE, Kingdon CC, Townsend PA. Spectroscopic determination of leaf morphological and biochemical traits for northern temperate and boreal tree species. Ecol Appl. 2014;24(7):1651–69. https://doi.org/10.1890/13-2110.1.
219. Zhang C, Atherton J, Peñuelas J, Filella I, Kolari P, Aalto J, et al. Do all chlorophyll fluorescence emission wavelengths capture the spring recovery of photosynthesis in boreal evergreen foliage? Plant Cell Environ. 2019;42(12):3264–79. https://doi.org/10.1111/pce.13620.
220. Huemmrich KF, Campbell P, Vargas ZSA, Sackett S, Unger S, May J, et al. Leaf-level chlorophyll fluorescence and reflectance spectra of high latitude plants. Environ Res Commun. 2022;4(3):035001. https://doi.org/10.1088/2515-7620/ac5365.
221. Yoshida Y, Joiner J, Tucker C, Berry J, Lee JE, Walker G, et al. The 2010 Russian drought impact on satellite measurements of solar-induced chlorophyll fluorescence: insights from modeling and comparisons with parameters derived from satellite reflectances. Remote Sens Environ. 2015;166:163–77. https://doi.org/10.1016/j.rse.2015.06.008.
222. Li Y, Zhang W, Schwalm CR, Gentine P, Smith WK, Ciais P, et al. Widespread spring phenology effects on drought recovery of Northern Hemisphere ecosystems. Nat Clim Change. 2023;13(2):182–8. https://doi.org/10.1038/s41558-022-01584-2.
223. Liu J, Cheng F, Munger W, Jiang P, Whitby TG, Chen S, et al. Precipitation extremes influence patterns and partitioning of evapotranspiration and transpiration in a deciduous boreal larch forest. Agric For Meteorol. 2020;287:107936. https://doi.org/10.1016/j.agrformet.2020.107936.
224. Damm A, Haghighi E, Paul-Limoges E, Van Der Tol C. On the seasonal relation of sun-induced chlorophyll fluorescence and transpiration in a temperate mixed forest. Agric For Meteorol. 2021;304–305:108386. https://doi.org/10.1016/j.agrformet.2021.108386.
225. Zhou K, Zhang Q, Xiong L, Gentine P. Estimating evapotranspiration using remotely sensed solar-induced fluorescence measurements. Agric For Meteorol. 2022;314:108800. https://doi.org/10.1016/j.agrformet.2021.108800.
226. Hennessey TL, Freeden AL, Field CB. Environmental effects on circadian rhythms in photosynthesis and stomatal opening. Planta. 1993;189(3):369–76. https://doi.org/10.1007/BF00194433.
227. Xiao J, Fisher JB, Hashimoto H, Ichii K, Parazoo NC. Emerging satellite observations for diurnal cycling of ecosystem processes. Nat Plants. 2021;7(7):877–87. https://doi.org/10.1038/s41477-021-00952-8.
228. Stavros EN, Schimel D, Pavlick R, Serbin S, Swann A, Duncanson L, et al. ISS observations offer insights into plant function. Nat Ecol Evol. 2017;1(7):0194. https://doi.org/10.1038/s41559-017-0194.
229. Qiu B, Xue Y, Fisher JB, Guo W, Berry JA, Zhang Y. Satellite chlorophyll fluorescence and soil moisture observations lead to advances in the predictive understanding of global terrestrial coupled carbon-water cycles. Glob Biogeochem Cycles. 2018;32(3):360–75. https://doi.org/10.1002/2017GB005744.
230. Rodriguez-Fernandez N, Barbier M, Verrelst J, Lindqvist H, Bueechi E, Munoz PR, et al. Paving the road to flex and biomass: the land surface carbon constellation study. In: IGARSS 2022 - 2022 IEEE International Geoscience and Remote Sensing Symposium. Kuala Lumpur, Malaysia: IEEE; 2022. pp 5571–5574. Available from: https://ieeexplore.ieee.org/document/9884465/.
231. Cook B, Corp L, Clemens P, Paynter I, Nagol J, McCorkel J. Characterization of firefly, an imaging spectrometer designed for airborne measurements of solar-induced fluorescence. In: IGARSS 2018 - 2018 IEEE International Geoscience and Remote Sensing Symposium. Valencia, Spain: IEEE; 2018. pp 3943–3946. Available from: https://ieeexplore.ieee.org/document/8518303/.
232. Woodgate W, van Gorsel E, Hughes D, Suarez L, Jimenez-Berni J, Held A. THEMS: an automated thermal and hyperspectral proximal sensing system for canopy reflectance, radiance and temperature. Plant Methods. 2020;16(1):105. https://doi.org/10.1186/s13007-020-00646-w.